Liu M. X. (Orcid ID: 0000-0001-7495-5270)
Pelosi A. (Orcid ID: 0000-0002-2306-5793)
Guala M. (Orcid ID: 0000-0002-9788-8119)

A statistical description of particle motion and rest regimes in open-channel flows under low bedload transport

M. X. Liu[1, 2] A. Pelosi[3], and M. Guala[2]†

[1] North China University of Water Resources and Electric Power, School of Water Conservancy, Zhengzhou, China

[2]Saint Anthony Falls Laboratory, Department of Civil, Environmental and Geo-Engineering, College of Science and Engineering, University of Minnesota, Minnesota, United States

[3] Department of Civil Engineering (DICIV), Università degli Studi di Salerno, Italy

† Corresponding author: Michele Guala

Key Points:

- The alternation between motion and rest regimes of sediment particles is observed under low bedload transport.
- Particle waiting times are classified into “active” and “deep” and their distributions are quantified experimentally.
- The particle waiting time decreases with increasing shear velocity, whereas the particle velocity, step length, and acceleration variance increase.

This article has been accepted for publication and undergone full peer review but has not been through the copyediting, typesetting, pagination and proofreading process which may lead to differences between this version and the Version of Record. Please cite this article as doi: 10.1029/2019JF005140

Abstract

In the last decade several efforts were devoted to model sediment-particle transport in rivers as a stochastic process. Experimental observations are therefore needed to validate these models and to provide the correct probability distribution of selected stochastic variables. The kinematics of sand particles is investigated here using non-intrusive imaging to provide a statistical description of bedload transport under incipient motion conditions. In particular, we focus on the alternation between motion (particle steps) and rest regimes to quantify the probabilistic distribution of the particles waiting time, which is suggested by many studies to be responsible for anomalous diffusion. The probability distributions of the particle step time and step length, streamwise and spanwise velocities, acceleration, and waiting time are quantified experimentally. Results suggest that variables describing the particle motion regime are thin-tailed distributed, whereas the waiting times exhibit a power-law distribution. A specific class of waiting times during which the grain is observed to oscillate without a net displacement is classified as active and is analyzed separately from the other, so-called deep waiting times. The experimental results, obtained under five different transport conditions, describe grain-scale kinematics and dynamics at different wall shear stress. They provide both a benchmark dataset for validating particle-transport numerical simulation and critical input parameters for the stochastic modeling of bedload transport.

1 Introduction

Bed load is a common mechanism of sediment transport for sand particles in natural flow, characterized by cyclic sequences of particles moving and resting on the sediment bed. [e.g. *Roseberry et al., 2012; Furbish et al, 2012; Lajeunesse et al, 2010; Fan et al., 2014, 2016; Gonzales et al. 2017*]. The physical mechanisms governing bed-load transport are highly complex due to (i) the turbulent fluctuations of the flow and (ii) random interactions of grains with each other and with the bed, over a wide range of bed topography and corresponding flow scales, from the grain size to the reach [e.g. *Furbish et al, 2012b*]. These circumstances make the nature of particle trajectories random itself and the bed-load transport highly variable in time and space, in particular at low flow rates [*Ergenzinger, 1988; Ancey, 2010*]. For such reasons, following the pioneering work of Einstein [1950], who introduced the probabilistic description of particle motion, recent efforts have been carried out to properly describe the motion of sediment particles transported in the proximity of the bed as a stochastic process [*Weeks et al., 1996, Ancey et al., 2006; Schumer et al., 2009, Ancey, 2010, Foufoula- Georgiou and Stark, 2010, Touchette et al., 2010; Bradley et al., 2010; Baule and Sollich, 2012, Furbish et al., 2012a; Furbish and Schmeeckle, 2013; Fan et al., 2014, 2016; Ancey and Heyman, 2014, Pelosi et al., 2014, Zhang et al., 2014, Ballio et al. 2018*]. The stochastic approach is computationally more efficient compared to high-fidelity direct numerical simulations of fluid and particle flows [*Schmeeckle and Nelson*, 2003, *Escauriaza and Sotiropoulos*, 2009, 2011; *Bialik et al*., 2012; *Durán et al*., 2012; *Schmeeckle et al*., 2014; *Gonzales et al*. 2017], but requires input distribution parameters. Experimental data on single particle motion have thus become fundamental to inform those stochastic models. Considerable experimental research has been focused on the quantitative description of individual particle motion [among others: *Niño and Garcia, 1996; Lajeunesse et al., 2010; Roseberry et al., 2012; Ancey and Heyman, 2014, Campagnol et al 2013, 2015*], leading to a statistical description of particle velocities, hop or step distances, associated travel or step times and waiting times, ultimately providing data for the calibration of stochastic models [see, e.g., *Papanicolaou et al., 2002, Furbish et al. 2012, Fan et al., 2014, 2016; Schumer et al., 2009*].

Some existing findings on the probability density functions (PDFs) of particle-scale kinematic variables, such as velocity, step length and waiting times are summarized here:

1) The PDF of the streamwise component of the particle velocity (u_p) has been mostly characterized by thin tails: the exponential distribution was recognized by *Lajeunesse et al.* [2010], *Roseberry et al.* [2012] and *Houssais et al.* [2012], though it is not clear if this is true only for the tail or also for the entire range of velocity values; Gaussian distributions were observed, among others by *Martin et al.* [2012], *Ancey and Heyman* [2014] and *Heyman et al.* [2014].

2) Several studies considered thin-tailed distributions for the step distance L_s and step times T_s , suggesting both the exponential distribution [*e.g.*, *Einstein*, 1937, 1950; *Sayre and Hubbell*, 1965; *Schmidt and Ergenzinger*, 1992; *Habersack*, 2001; *Wu and Yang*, 2004; *Fan et al*. 2016] and the gamma distribution [*e.g.*, *Yang and Sayre*, 1971; *Lajeunesse et al*., 2010], as opposed to the heavy-tailed distributions proposed by *Bradley et al*. [2010] and *Ganti et al.* [2010]. In particular, the last study showed analytically how a heavy-tailed distribution for particle step length arises in a sediment mixture where exponentially distributed step lengths are assumed for each grain size.

3) When a particle stops, little is known about its resting/waiting time (average value variability, distribution). To assess the PDF of the particle resting/waiting time, hereafter referred to as T_w, several measurements were performed under very different hydraulic conditions, bed material composition, and methodology, both in the laboratory [*Wong et al.*, 2007; *Martin et al.*, 2012; *Heyman et al.*, *2013; Martin et al.*, 2014, *Cecchetto* et al. 2018] and in the field [*Olinde and Johnson*, 2015], resulting in waiting-time distributions' tails ranging from heavy to thin according to the prevailing factors, as we discuss in Section 5.

The high interest in the assessment of those PDFs for particle-scale kinematic variables lies in the circumstance that particle dispersal and, in particular, the diffusion exponents of the stochastic process describing particle motion may relate directly to the parameters of the probability distributions of particle motion characteristics, such as step lengths and/or waiting times [*Nikora et al.*, 2002; *Schumer et al*, 2009b: *Ganti et al.*, 2010; *Pelosi et al.*, 2014]. For instance, it has been suggested that, if the probability density functions of u_p, L_s, T_s and T_w are all thin-tailed, the resulting particle diffusion regime is always normal for all scales [*Han and He*, 1980], except for super-diffusion at very short initial time scales due to particle inertia, i.e. ballistic motion [*Nikora et al*., 2002; *Fan et al*., 2014; *Mo and Raizen*, 2019]. Following seminal works by *Week* et al. [1996] and *Schumer* et al. [2009b], recent simulations by *Fan et al*. [2016] showed that the anomalous sub-diffusion of bed load particles can arise from the thick-tailed distribution of the waiting times [see also *Ganti et al.* 2010 and *Pelosi et al*. 2016]. In this context, the need to collect more experimental data both from the laboratory and the field in order to achieve a deeper understanding of particle transport at the grain scale is apparent. First, we aim to estimate probability density functions (PDFs) of particle-scale kinematic variables, such as velocity, acceleration, step and waiting times, and their dependence on the bed surface shear stress. The second objective is to understand better the link between the variability in the waiting-time distribution function, and related tails, and the forces acting on the grains, with some emphasis on turbulence-induced drag and the frictional forces resulting from the interaction with the bed surface.

The experimental challenge is to focus on both the temporal domain and the spatial domain, in which particles are identified as active (moving) or passive (resting). With this purpose, under low transport and for a flat bed, a Lagrangian description of sediment kinematics **is** employed. This approach may be advantageous (i) to identify key time scales of

the forces acting at the grain scale and their potential relation to known turbulent time scales, and (ii) to predict statistical properties of the advection and dispersion of an ensemble of particles, all requiring a predictive understanding of the time spent by a particle resting on the bed surface [see e.g. Fan et al. 2016, Gonzales et al., 2017]. The PDFs of resting times T_w, to the best of our knowledge, have been quantified experimentally under very different transport and hydraulic conditions [*Wong et al.*, 2007; *Martin et al.*, 2012; *Hassan et al.*, 2013; *Heyman et al*. 2013 and *Olinde & Johnson* 2015, *Cecchetto et al.* 2018], which are compared in more detail in our discussion section. Some of the reasons why experimental results show different trends and distribution, in particular for the waiting time, involve both technical limitations and the overlap of various interconnected transport mechanisms occurring under different shear stress, hydraulic conditions, and bedform evolution. The intrinsic limitations in the spatial or temporal domain size of the sand-grain kinematics measurements are known to prevent a robust analysis on the tails of the particle velocity or step-length distribution [*Phillips et al*., 2013, *Martin et al*., 2014]. While we acknowledge this limitation in our work, we also recognize a recent approach that could mitigate this problem [*Ballio* et al., 2019]. Another potential source of variability is the effect of sediment-mixture heterogeneity [*Houssais and Lajeunesse* [2012], which could be related to the different waiting-time distributions proposed in the literature. All of these issues are important for the physical understanding of sediment-transport mechanisms, for the correct prediction of particle trajectories (micro-scale), and for the advection and diffusion properties of the particle ensemble (macro-scale), as discussed above [*Han and He*, 1980, *Nikora et al*., 2002; *Fan et al*., 2014, *Week* et al., 1996, *Schumer* et al 2009b, and *Fan et al*. 2016]

In this contribution we investigate the kinematics of natural sand particles moving on an erodible bed in the absence of bedforms. Recent experimental advancements, enabling underwater imaging at affordable costs, allow us to monitor particle motion at high spatial and temporal resolutions. Such measurements have been performed and are presented here to study particle transport under five different hydraulic conditions and shear-stress intensities, covering the transition from incipient motion to bed-load transport over a flat surface. With specific reference to the cyclic sequence of step and resting times of the sediment grains, we focus on the distribution of particle velocities, accelerations, step and waiting times, and on the joint probability distribution of particle hop distances and associated travel times. Particular emphasis is given to the waiting times, their identification, and proposed classification. In order to provide also a phenomenological picture of particle motion, we further investigate the accelerating and decelerating regimes of particles using Lagrangian statistics, which are critical for the correct modeling of the forces acting on the particles.

2 Laboratory experiments and measurements

2.1 Experimental apparatus

The experiments were conducted in a 15-m-long rectangular flume in the St. Anthony Falls Laboratory at the University of Minnesota. Different hydraulic conditions were tested under low bedload transport (see Table 1). Near-bed longitudinal (u) cross stream (v) and vertical (w) instantaneous velocities were measured with an acoustic Doppler velocimeter (ADV) sampling at 200Hz an observation volume located 0.015 m above the bed surface. The shear velocity $u_* = \sqrt{-\overline{u'w'}}$ was estimated using the velocity fluctuations u' and w' at the measurement location and compared with the estimate based on the logarithmic fit of the mean velocity profile. An 8% underestimation was calculated, and compensated for, in the

$u_* = \sqrt{-\overline{u'w'}}$ estimate. The Froude number, $Fr=U/(gh)^{1/2}$, based on the mean cross sectional velocity U and flow depth h, varied from 0.27 to 0.30. The mean cross sectional velocity is quantified as $U=Q/Bh$, where Q is the flow discharge and B=0.9 m is the channel width. Experiments S1 to S5, described in Table 1, were designed to explore a range of low-bedload-transport conditions without generating bedforms. The Reynolds number, $Re=Uh/\nu$, where ν is the kinematic viscosity, varied from 38,700 to 50,300. The Shields number $\theta = \frac{u_*^2}{(\rho_s/\rho - 1)gD_{50}}$ varied from 0.021 to 0.040. The sediment particles used in all experiments are from a coarse quartz sand mixture with uniform gradation, and a median diameter D_{50} = 1.1 mm (D_{20} = 0.9 mm, D_{80} = 1.4 mm). The sand and water densities are ρ_s = 2650 and ρ = 1000 Kg m^{-3}, respectively. The hydraulic flow conditions in our first experiment were imposed to be at the lower limit of critical mobility. This was achieved using visual underwater inspection at the channel test section. Along with particle video capturing, we measured flow discharge, depth and slope of the free surface to obtain a reliable estimate of the shear velocity. In the following experiments, we changed in small steps the flow discharge (in both directions) to cover a range of transport conditions, with the specific constraint to not induce bedforms. To ensure minimal disturbances on the surface, before each experiment the erodible bed was flattened with a plate board, to be parallel to the prescribed channel slope, and the water level and discharge were raised very slowly. The observing time of each experiment was limited to 20 minutes, under which the bed surface in the channel test section was observed to remain flat. Following the water drainage from the channel we never observed any bedform or geomorphic features in the test section.

In the range of episodic surface-particle transport to low bed-load transport, as monitored here, physical scaling arguments suggest that video length should not be based necessarily only on the channel flow spatio-temporal domain, but rather on the particle-scale kinematics. Based on velocity measurements, 20-second videos represent 100–200 integral time scales of the flow, and about 200 particle step times (defined as the time in which the particle is moving without a stop or rest). Anticipating some of the results presented below, a 6-cm (0.06-m) observation volume represent 60 particle diameters and about 10 times the average step length. Therefore, the extent of our spatio-temporal domain is considered wide enough in all relevant dimensions to cover the particle kinematics in the range of conditions explored here. Under higher transport with migrating bedforms and/or an active thick layer of sediment experiencing burial and entrainment events, the quantification of the particle waiting time would need a different approach, like the one originally pursued by *Wong et al.* [2007] and *Pelosi et al.* [2014, 2016].

2.2 Particle tracking

A slightly submerged camera was used to image the bed surface at 120 frames per second over a 6.3–7.3 cm (stream wise) × 4.7–5.5 cm (spanwise) domain with 640×480 pixel resolution. Those videos provided the image datasets for tracking particle motion. The field of view was illuminated by a downstream-located halogen lamp equipped with a lighting reflector paper to diffuse the light and to reduce background image fluctuations due to free-surface undulation. Videos of particles transported as bedload and actual trajectory data can be accessed in the supplementary material accompanying this paper (see also the acknowledgements section). The full dataset comprises 26–34 videos for each of the five shear-stress conditions. The duration of each video is 20 s (2400 frames, spaced by 0.0083 s), which is enough to provide a detailed description of the particles' step-and-rest intermittent motion.

The code for detecting and tracking particles is based on Matlab image tools. First, we employ a feature detection and extraction algorithm to record the coordinates of each active particle moving across successive frames. The functions ForegroundDetector and BlobAnalysis are used respectively to separate the background from the moving particle in the foreground and to connect the identified foreground objects, i.e., the moving particle. The foreground detection is completed using a two-dimensional Gaussian filter model. For each area detected in motion and thus identified as a particle, we estimated the centroid in each frame to specify its (x_p, y_p) position. The centroids of each active particle as it moved within successive frames were marked and converted to streamwise and cross-stream coordinate positions, respectively. The second algorithm is designed to identify the positions of corresponding active particles between different frames. The metric we used to link particles between successive frames include the displacement angle with respect to the streamwise direction and the maximum distance, as well as the history of the particle motion. For each particle, comparative links are attempted for a number of neighboring target particles in the next time frame: the optimal link is based on the projected position according to the actual particle velocity, when available (minimal acceleration), or on a nearest neighbor. Additional constraints to guide our tracking involve (i) maximum particle velocity not to exceed the mean flow velocity U_m measured by the ADV at roughly four particle distance from the wall; (ii) maximum particle acceleration not to exceed $\frac{1}{2}U_m$ in one Δt*;* (iii) backwards particle motion not to exceed 1/10 of the particle diameter in one time step Δt . Once particles are linked, the streamwise and cross-stream displacement of each particle linked in a trajectory are estimated $\Delta x_p = x_p(t + \Delta t) - x_p(t)$ and $\Delta y_p = y_p(t + \Delta t) - y_p(t)$ between frames. From the displacements, we estimated the instantaneous particle-velocity components $u_p = \Delta x_p / \Delta t$ and $v_p = \Delta y_p / \Delta t$, where Δt = 0.0083 s is the sampling interval. From all the particles that moved at some point over the entire duration of 32 videos (e.g., for Exp. case S1), we identified a datasets of 20684 unique spatial coordinates organized in 261 particle trajectories. The entire duration of 57 videos (experimental case S2, S3) formed a dataset of 58543 unique spatial coordinates (816 particle trajectories). Experiments S4 & S5, characterized by higher transport, contributed to more than 90658 spatial coordinates (1989 particle trajectories). A significant number of particles were not linked in trajectories due to tracking ambiguities, or to particles exiting the field of view at the beginning of the recording, or entering the field of view at the end of the recording. In particular, the missing links contribute to break a trajectory into smaller disconnected sections, where velocity and acceleration become less reliable and which require a strict vetting process. Some details on the vetting of particle trajectory are included below and in Table 2: The total number of the particle trajectories is N_{raw}. The particle trajectory with an integrated displacement less than $5*D_{50}$ were discarded. The number of particle trajectories left is N_{gt}. This represents a reliable dataset for particle velocity and acceleration. However, aiming at investigating the waiting time, we further and significantly restricted the whole datasets to long particle trajectories, with integrated displacement over 10 D_{50}, and experiencing at least one step-stop-step sequence of motion and rest. The final number of the trajectory selected is reported as N_s. To avoid unrealistic particle links from frame to frame, all N_s particle trajectories were inspected visually in the temporal and spatial domain. We acknowledge that there are unavoidable uncertainties in the automated particle-tracking process. However, the uncertainties and tracking ambiguities decrease when the mean inter-particle distance in the spatial domain is much smaller than the mean particle travel length from frame to frame. Thus, to monitor optically the ensemble motion of particles, increase in bed shear stress controlling particle activity and thus the inter-particle distance must be counter-balanced by an increase in the acquisition frame rate. This constraint set the limits of our higher-shear-stress experiment. However, linking moving particles into trajectories was not the only challenge we had to

face: in order to determine the sequence of hops (or steps) and resting (or waiting) times of bedload particles, we had to be very careful in the definition of particle "in motion" as opposed to particle "at rest". In the low-transport regime investigated here, many particles were observed to oscillate back and forth without contributing to net streamwise displacement. Although particles travelled downstream, some particles moved upstream instantaneously ($u_p < 0$), likely due to the rocking motion before the actual hop. To account for all these uncertainties, a cutoff (streamwise) velocity u_c=0.015 m/s was selected, corresponding to a displacement of about 1/10 of the particle diameter in one Δt, as reported above. We then defined a particle with $u_p < u_c$ to be at rest. Conversely, a particle is considered to be in motion if $u_p \geq u_c$.

2.3 Quantification of positioning velocity and acceleration error

Our tracking algorithm detects the moving particle as a coherent, finite sub-image region where pixels change their intensity compared to the local background. In particular, the outcome of the tracking procedure, in addition to the centroid, provides the streamwise and spanwise extent of the particle image region, which can be used to estimate an equivalent particle diameter. Because of the sand grains' complex geometry and its orientation variability, the projected shape, light reflection, and two-dimensional image of every particle change as the particle moves through each frame in sequence. Since the particle diameter physically cannot change, we can estimate the error in the positioning as a function of the standard deviation (D') of the equivalent diameter along a trajectory (see Figure 1). Specifically, we infer that the maximum error in the true centroid location is $\frac{1}{2} < D' >$, where the averaging operator is performed along many trajectory portions where the particle is considered to be in motion. Figure 1(b) shows the variability of one particle equivalent diameter along a trajectory.

To reduce this uncertainty in true centroid locations, a light diffuser was added to render the light more uniform and avoid excessively bright pixels within the true particle outlines; this allowed increasing the average size of the detected area of the particle up to the true size of the median particle D_{50}=0.0011 m, which was obtained through progressive sieving of the flume bed material. In Figure 1(b), D' is estimated to be about $0.11D_{ave}$, where D_{ave}=1.25 mm is the average diameter of the particle along the very same trajectory: the error, approximately 5.5% D_{ave} =0.07 mm, is in our opinion acceptable. The displacement error propagates as velocity and acceleration errors of 0.0084 m s^{-1} (about half of the cutoff velocity u_c) and 1.008 m s^{-2}, respectively. There are other sources of error that result in a reduced ability to link particles into a trajectory. First, there may be two or more target areas recognized on the projected surface of the same particle. The minimum diameter of the object recognized as a particle is set at 0.25mm, which is a compromise between the requirement to identify dimly illuminated particles and the one to avoid independent recognition of the same particle leading to tracking ambiguities and significant errors in velocity estimates. A second solution to limit errors associated with centroid ambiguities due to multiple target areas was to filter out trajectories based on the total displacement, integrated along the full trajectory, as mentioned above, and then filter out steps smaller than half of the particle radius ($L_s < D_{50}/4$). The last procedure, implemented to avoid error propagation in the particle motion statistics, consists of a smoothing filter applied to the particle velocities along the trajectory, thus in the Lagrangian time coordinate. This operation was performed on the limited subsets of long trajectories (N_s) that were also visually inspected one by one, representing the core of our processed datasets (see Table 2). This sequence of data vetting and validation is very costly in terms of actual loss of information, but it is necessary to provide long trajectories and reliable

statistics. Figure 2 illustrates an ensemble of particles tracked over the field of view in one video recording.

2.4 Definition of particle steps (motion) and rests (waiting time)

Figure 3 shows a spatio-temporal sequence of steps and resting states of a single particle transported on the bed surface. From a purely spatial reconstruction of the trajectory we cannot clearly define the periods in which a particle is moving (step or hop) or resting. Therefore, such a distinction has to be made based on the temporal evolution of the particle velocity. Here we chose the streamwise velocity component to define the step time T_s and the waiting times T_w. Accordingly, we can define also the step length L_s as the distance covered by the particle in each step time. The conditions defining the particle's step and waiting regimes are based on (1) a cutoff velocity, above which the particle is considered in motion, and (2) a finite integrated streamwise displacement exceeding $D_{50}/4$, which is required to treat the rocking, oscillatory motion of particles with finite velocity, but no net displacement, as a contribution to the waiting time. We tested a range of cutoff velocity values (0.005 m/s, 0.01 m/s, 0.015 m/s, 0.018 m/s, and 0.02 m/s) to quantify their effects on the definition of the particle waiting and step times. After comparing statistics of the average waiting times for each cutoff velocity, and after visual inspection of all the selected instantaneous trajectories (as depicted in Figures 2 and 3), we identified an optimal range of 0.01–0.015 m/s. This is consistent with the cutoff velocity of 10–30 mm/s adopted by [*Lajeunesse et al.*, 2010]. We eventually picked a threshold value of 0.015 m/s, which corresponds to about twice the error that we estimated due to particle centroid uncertainty. Note that (i) the velocities of particles were filtered before estimating the step and wait period; (ii) each waiting time is delimited by two step times, never by the beginning or by the end of a trajectory or the video acquisition; and (iii) step time and step length potentially suffer from truncation bias effects due to particles entering or exiting the field of view.

3 Results

This section is structured to provide, first, results on the bedload particles in the motion regime, and later to present the statistics on the waiting times. The first subsection therefore will be focused on the streamwise and the spanwise components of the particle velocity, u_p and v_p respectively, on the step length L_s and step time T_s, and on streamwise component of the particle acceleration a_s. Because of the low number of moving particles detected at the lowest shear stress conditions S1 (see Table 2 and section 4), in this section we focus on the probability distribution of resting and moving particle properties for the experimental cases S2 to S5.

3.1 Statistical description of particles in motion

The distributions of the particle streamwise velocity component u_p for the different experimental conditions are presented in Figure 4. The tails of the reported PDF are, in all cases, following an exponential distribution. However, for low velocity values the distributions exhibit a shift in shape that was observed by *Lajeunesse et al.* [2010] but not by *Roseberry et al.* [2012], suggesting the use of a gamma function:

$$f_u(u) = \frac{1}{b^a \Gamma(a)} u^{a-1} e^{\frac{-u}{b}} \qquad (1)$$

where, a and b are parameters with a > -1, and b > 0, and Γ is the gamma function. When a=1, $\Gamma(1)=1$ and Equation (1) reduces to an exponential distribution.

We argue this change in shape partially depends on the above definition of rest and motion regimes. In particular, if we consider all the non-zero particle velocities, including both the motion and the ambiguous rocking back-and-forth state, the velocity distributions maintain the exponential trend in a lower range, and show a finite probability for negative velocities, observed by *Roseberry et al*. [2012] and interpreted here as the result of particles rocking. However, because we are very interested in quantifying the waiting times, we defined a non-zero, finite threshold velocity to mark the separation between motion and rest states; in this respect, we classify the particles in oscillatory motion as particles at rest, without contributing to the PDFs shown in Figure 4, since they do not experience a net streamwise displacement. Particle-size heterogeneities may be another cause for this trend, since the PDF(u_p) calculated on our data is similar to the distribution provided by *Houssais and Lajeunesse* [2012], estimated in a bimodal sediment bed. Because the distribution is a thin-tailed gamma function, the mean particle velocity is well defined, converging to its real value under the given observation time. With weakly increasing shear velocity u_* , from experimental conditions S2 to S5, $<u_p>$ increases slightly from 0.067 to 0.086 m s^{-1}. It seems reasonable that the shear velocity is the relevant scale for the particle velocity, since both quantities are related through a sediment mass flux formulation. The ratio between the particle and the shear velocity is in fact only weakly varying, with u_p/u_*= 3.1~3.5. This is in agreement with known formulations describing u_p=C(u_*-u_{*c}) with C in the range 13.4–14.3 (*Abbot and Francis* [1977]) and 6.8–8.5 (*Nino et al.*[1994]), compared to our average C=12.6 with estimated values between 9.8 and 14.2 (see also a recent review by *Ali and Dey* [2019]).

We observe that the PDF of the cross-stream particle velocity v_p is symmetric and could be well described by a Gaussian function centered on zero, as shown in Figure 5, consistent with the experimental results of *Lajeunesse et al*. [2010]. However, the tails of the distribution depart from the Gaussian function and resemble an exponential function, as suggested by the experimental result of *Roseberry et al*. [2012]. A transition between these two distributions is observed under all the experimental conditions, for cross-stream velocity values larger than $|v_p|$> 0.1m s^{-1} so it appears to be a genuine feature of this dataset. Note that the r.m.s. (root mean square) streamwise and spanwise particle velocity components are $u_{p\,\mathrm{rms}}$ =0.044, 0.051, 0.052, 0.054; $v_{p\,\mathrm{rms}}$ = 0.029, 0.032, 0.033, 0.038, which are a fairly consistent, scaled representation of the local streamwise and spanwise fluctuating velocities in the corresponding rough wall turbulent boundary layer. In particular, from ADV measurements, we estimated at a vertical location z/D_{50} =13.6 the root mean square flow velocities u_{rms} = 0.050, 0.053, 0.055, 0.061 and v_{rms} =0.037, 0.038, 0.043, 0.045, leading to u_{rms}/v_{rms}=1.36, 1.39, 1.27, 1.33. These values are just slightly smaller than $u_{p\,\mathrm{rms}}/v_{p\,\mathrm{rms}}$=1.52, 1.59, 1.58, 1.42, which are, however, estimated closer to the bed surface, confirming that turbulent motions have a strong effect on the particle velocity variability [see e.g. *Niño* and *Garcia*, 1996]. The other source of particle velocity variability would be the interaction with the resting particles at the bed surface.

The distribution of particle acceleration is plotted in Figure 6. Due to the exponential distribution of the particle velocity, we expect and observe a Laplacian distribution of streamwise acceleration. The form of the function is:

$$f(a_s|\mu,b) = \frac{1}{2b}\exp\left(-\frac{|a_s-\mu|}{b}\right) \qquad (2)$$

where μ is the location parameter and is estimated with the median value of a_s (reported in the range of 0.23 to 0.33, thus close to the expected value of zero, given the wide range of acceleration values), and b is the scale parameter estimated as < abs(a_s - μ) >. The values of the two parameters are provided in the caption of Figure 6. It is noteworthy that the

standard deviation of the streamwise acceleration a_{rms}, as well defining the width of the distribution, increases with the shear velocity from 4.4 to 5.2, 5.4, 6.1 ms^{-2}, for the four cases respectively. From a dimensional perspective we can normalize the acceleration with u_*/T_s, leading to $a_{rms}\ T_s/u_* = 26.4, 29, 29, 29.7$ (see Section 4).

The distributions of step (or travel) time T_s and step length L_s of moving particles are plotted in Figures 7 and 8 respectively, for all four cases. All the PDFs show consistently the thin tails of the exponential distribution, which allows us to reasonably compare averaged values, for increasing shear velocity and mass flux. The mathematical form of the distribution is $f_x(x) = \frac{1}{\lambda} e^{-x/\lambda}$, where x refers to T_s or L_s, and the only parameter is the mean value (provided in the captions of Figs. 7 and 8). In particular, we note that the travel time does not change significantly with u_* for the range investigated, suggesting that the increased mass flux is more correlated to an increase in particle velocities, and a decrease in waiting time, as discussed later, rather than to an increase in the step time. In fact, the average step length $<L_s>$, which is expected to converge thanks to the exponential thin-tailed distribution of L_s shown in Fig. 8, increases slightly with u_*, proportional to the increase in $< u_p >$. Note that the shape of the histogram of L_s in our experimental results is more consistent with the one reported by *Lajeunesse et al*. [2010] than with that repoted by *Roseberry et al*. [2010], where the distributions are approximated as a gamma function.

The step length and time were observed to be correlated and jointly distributed following a power law [Roseberry *et al*., 2012; *Fan et al*., 2014]. Our results confirm the power law distribution for varying shear velocity, but on a slightly different exponent (Fig. 9). The various groups were fitted by an exponent in the range of 1.25–1.29, as compared to 5/3 ~ 1.67 found by *Roseberry et al*. [2012], and plotted for comparison (22–25% difference). Because of the weak dependence between L_s and u_*, the power-law exponents are gently decreasing with increasing transport rates. The difference between our and *Roseberry et al*. [2012] results might be attributed to our slight heterogeneity in the particle-size distribution [see *Houssais and Lajeunesse*, 2012]. Note that the step-length distributions can be heavy-tailed, with power law decay arising from heterogeneity in grain sizes and other complexities in natural bed sediment [*Ganti et al*., 2010].

3.2 Lagrangian description of moving particles

The description of bedload transport in terms of step length, step time, and particle velocity is consistent with an Eulerian reference system, in which a fixed observer is monitoring the moving particles. An alternative description of bedload transport can be provided by looking at the particle velocity along the trajectory, as a function of the Lagrangian time τ, starting at $\tau = 0$ when the particle begins a step. Visual examination of particle velocities along trajectories revealed a fairly common trend, showing that particles experienced high velocity at the beginning of their trajectory that then decreased slowly. To provide a statistical representation of this trend we perform an average of the streamwise velocity conditioned on the travel (Lagrangian) time τ, i.e., on the time frame since the beginning of the step (Fig. 10a). In the ensemble we only include trajectory portions longer than 0.15 s in which particles are moving, thus with no effects from the waiting time and no selection-bias effects due to shorter trajectories. The limiting choice of the maximum τ resulted as a compromise between the need to include a sufficient number of long trajectories in the conditional averaging (in this case 60) and the need to describe statistically a segment of the particle motion on the same order of the averaged step time. In Figure 10 we included results from

two different sets S4 and S5; due to increasing transport rate, the S5 set had longer trajectories and we could extend τ up to 0.24 s. The averaging operation performed on the streamwise acceleration results shows that the particle first experiences a sudden streamwise force when it is accelerated and entrained into the flow and then a gentle but more persistent drag as it slows down (Fig. 10b). This asymmetry in the Lagrangian history of particle velocity and acceleration suggests that the first particle displacement in the step could be caused by an energetic event, e.g. a particle-particle collision [see, e.g. *Frey and Church*, 2011] or a strong sweep event (thus a local streamwise drag [see e.g. *Nino and Garcia*, 1998]). The slightly negative acceleration slowing down the particle velocity before rest could be due to either (i) the ejection events, following sweeps, combined with the higher inertia of the solid particle maintaining a velocity larger than the surrounding fluid, and inducing fluid drag acting now in the opposite direction, or due to (ii) frictional contacts with the particles on the bed surface. Note that the switch in the sign of the acceleration, potentially corresponding to the end of the ballistic regime, occurs at approximately τ = 0.05–0.1s, leading to a dimensionless Lagrangian time $\tau u_* / d_s$ ~1–2. This is in very good agreement with the results by *Campagnol et al.* [2015], thus supporting the frictional rough wall turbulence scaling and its effect on particle transport.

3.3 Statistical description of resting particles

The waiting, or resting time, plays a key role in relating the intermittent particle kinematics to the actual sediment transport rate and mass flux, in particular under low bedload transport conditions. In order to quantify waiting time statistics and their probabilistic distribution unequivocally under a limited spatio-temporal observation domain, we rely on particles that, in their trajectory, are classified as in *motion state* before and after the *resting state*, as shown in Figure 3. However, as previously discussed, particles often oscillate back and forth, and thus exhibit a non-zero velocity, when they stop in a specific location without contributing to net displacement. We define those as *active* waiting times, in the sense that the particle is still actively moving but not contributing to the mass flux. In other cases, both the particle velocity and their streamwise net displacement are zero, implying that the particle has clearly stopped and the trajectory is interrupted; these are referred to as *deep* waiting times, as sketched in Figure 11.

The deep waiting time identification may lead to some ambiguities because, if the tracking of one particle stops when the particle is at rest, we have to be sure that the next step begins with the very same particle in the very same location. In addition, we have to note that the estimates of deep waiting times are strongly conditioned by our limited sampling interval (maximum consecutive recording time of 20s); implying that we may face a significant selection effect. In the current analysis, we first show the distribution of the active waiting time, which is affected less by these limitations. The active waiting times are significantly shorter than the deep waiting times; the particle's oscillatory motion is indeed a signature of the local flow conditions approaching critical mobility, when weak turbulence fluctuations may be enough to entrain the particle in the flow again (see Table 1). Note that the cutoff velocity u_c has a weak effect on the waiting time classification: by varying u_c from 0.011 to 0.02 m s^{-1} in the S5 case the average active waiting time decreases from 0.16 to 0.14 s, whereas the deep waiting time increase from 3.18 to 3.54 s. The distinction between the active and deep resting states is based on the particle's probability of landing, or not, under relatively low turbulent flow conditions or in a sheltered spot within the bed surface; thus, it involves both flow and roughness heterogeneities. It is reasonable to expect that particles within the bed surface matrix are more difficult to entrain as compared to particles that remain exposed to the flow. This is one aspect of the armoring mechanism, for low bedload

transport, and could be sufficient to explain the difference between deep and active waiting times. In terms of turbulent flow heterogeneities, we speculate that a time scale of 0.1 s, consistent with the mean active waiting time, can be derived as a ratio of the particle diameter to the shear velocity D_{50}/u_* ~ 0.04–0.05 s; the latter is referred to as a representative time scale for near surface (rough wall) turbulent fluctuations, based on a measure of surface roughness heterogeneities ~ D_{50} and near wall velocity u_*. We also estimate the integral time scale of turbulence, from the streamwise velocity fluctuations measured by the ADV at z/D_{50}=13.6, in the range between 0.2 and 0.3 s, which can be interpreted as a separation time scales between consecutive sweeps, and covering multiple ejections events [*Sumer and Oguz*, 1978, *Rashidi et al.*, 1990; *Nino and Garcia*, 1996; *Tardu*, 2002]. The comparison of these time scales suggests that active waiting times predominantly depend on the turbulent forcing scales, with weaker effects from trapping or sheltering mechanisms due to roughness heterogeneities. The latter are inferred to influence the deep waiting times more significantly.

In all experimental cases, the distribution of the active waiting time T_{wa} is a power law function (see Equation (3) and Fig. 12). We estimated the power-law exponents, decreasing from b=-1.3 to -1.9 (for cases S2 to S5), suggesting that the tail thickness increases with decreasing transport rate and decreasing u_*. The tails of the power law distribution are expressed as:

$$f_{T_w}(T_w) = aT_w^b \qquad (3)$$

where, T_w denotes the waiting time, referring to T_{wa} and T_{wd}; a and b are parameters with a ~ 0.1. The estimated variations of the b exponent suggest that the lower the transport rates, the higher the probability of observing rare but very long waiting times, which contribute to increase the average active waiting times. It is important to stress that the above power-law exponents do not ensure the convergence of the mean values with respect to the total observation time, leading to a questionable estimate of $< T_{wa} >$ (Table 3). Note however that in the highest transport condition, T_{wa} exhibits a power law distribution with b= -1.9, which is very close to the convergence threshold exponent b=-2, suggesting that at any larger shear stress the average of the active waiting time would be independent of the observation time. The observed trend in the power-law exponent is amplified for the deep waiting times, with their distributions plotted in Figure 13. As expected, the PDF does not change mathematical form, with the exponents consistently increasing from -1.32 to around -0.83, with u_* decreasing. The latter values, in good agreement with the results from Cecchetto et al. [2018], unambiguously identify the thick tails of the distributions, thus compromising the statistical convergence of the mean (as well as the median, for b > -1). The first consequence is that average waiting times become more and more **dependent** on the amount of data collected and on the monitoring period. Therefore, the waiting time values provided for the sake of completeness in Table 3 must be taken with a lot of caution.

3.4 Waiting-time distribution between migration events

An Eulerian analysis was performed on the interval time between sequential particle migration events, defined by crossing a virtual target cross-section in the field of view. Following the procedure of *Heyman et al.* [2013] we defined the resulting waiting time associated with variation of the bedload flux as T_{wf}. as sketched in Figure 14. The red curve in Figure 14b identifies the k^{th} migration event, where N is the total number of particles crossing the target section during the k^{th} migration event (at least one particle should cross, $N \geq 1$). The blue line denotes the period with no migration events in the target cross-section. T_{wfk} is the waiting time of particle migration $T_{wfk} = S_k - S_{k-1}$, calculated as the interval time

between the k^{th} and $(k\text{-}1)^{th}$ migration events, S_k and S_{k-1} respectively. The probability distribution of T_{wf} is shown in Figure 15. Here, we only show results at two flow conditions, S2 and S4, with $u_* = 0.022$ and 0.024, respectively. In our experimental conditions, the shape of the T_{wf} distribution follows again a power-law function. It is relevant to note that the exponent decreases significantly from -1.23 to -2.14 as u_* increases from 0.22 to 0.24, which is much faster than the change of active waiting time T_{wa} with u_*. The rapid thinning of the T_{wf} tail suggests that the distribution of T_{wf} may evolve into an exponential function under high bed shear stress and intense transport, as proposed by *Einstein* [1950] and quantified by *Heyman et al.* [2013]. In the PDF of T_{wf} in Figure 15, we do not observed a time-scale separation marking a change in the distribution, as observed by Heyman et al. [2013]. The reason might be that we are still under low transport. The *Heyman et al.* [2013] experiments were conducted on a steep slope (7%) with shallow water and migrating bedforms. The latter, in particular, might affect the waiting-time distribution introducing (bedform) timescales that are not necessarily contributing to the core of the turbulent high-frequency spectrum responsible for bedload transport near critical mobility, and therefore change the probability of occurrence of instantaneously high shear stress at the bed. It is noteworthy that the shape of the waiting time distribution is confirmed, as compared to the active and deep waiting times. However, the exponent varies: the bedload flux waiting time is much closer to the active waiting time (for the S2 case they are within the range 1.55–1.39, in the S4 case the range is [1.97–2.14]). This could be a consequence of the fact that active and bedload-flux waiting times are estimated from particles that are either moving or oscillating, and thus well exposed to the fluctuating drag of the turbulent flow. The main difference is in the method, since T_{wf} does not require the identification of the resting section of a particle trajectory and thus is less sensitive to the velocity cutoff velocity threshold. The reasonable agreement between the T_{wf} and T_{wa} distributions partially supports our procedure.

4 Particle statistics under varying shear stresses

Experiments have been performed under varying shear velocities close to the Shields critical conditions. Additional preparatory experiments were conducted at lower shear stress, and the number of moving particles was recorded to identify unequivocally the threshold of motion for our bed-material composition (see Fig. 16 and note that the low number of particles reflects the strict trajectory-selection procedure). Specifically, the extrapolated shear velocity corresponding to the limiting case of no moving particles has been obtained as u_{*c}=0.0173. The resulting range of low bedload transport comprises u_*/u_{*c} between 1.1 and 1.5. Within this range, bedload transport can be described in terms of particle-scale kinematic properties as described in the Results section, above. Let us consider the S1 case as a reference and the S5 case as the most active one, likely to display the largest differences in the examined variable space. First we note from Table 1 that the particle step time T_s remains fairly invariant (~3%), as opposed to the particle step length L_s (40%) which in fact increases due to an increase in particle velocity u_p (33%). The increase in particle velocity is both sustained by higher mean velocity values (15% at z/D_{50}=13.6) and mostly by an increase in turbulence level manifested by the shear velocity, or more directly by the Reynolds stresses (44%). The increased turbulence perceived by the particle is also reflected in the increase standard deviation of the particle acceleration (28%). The mean active waiting time decreases substantially (29%), implying that particles, after a completed step, are more likely to be destabilized again with increasing shear stress, due to sweeping turbulent events. The deep waiting times are observed to be about 19–23 times longer than the active waiting times, under the total observation period investigated. They decrease by 14% under increasing shear stress (S2–S5), significantly less than the active waiting times (29% in the range). This is likely due to the fact that large deep waiting time values are not captured in our observation

period, and that deep waiting times may be more affected by the roughness heterogeneity of the bed and particle self-organization (e.g., *Sun et al*., 2015) and less dependent on the wall shear stress. The ratio of active to total waiting times (as number of events) increased from 34% (S2) to 39% (S3), 48% (S4), and 60% (S5).

However, the number of particles in motion on the bed, within the camera field of view, as observed in an Eulerian perspective, varied dramatically, with the particle activity increasing by more than 300% with increasing u_*. This means that our Lagrangian statistics do not provide an exhaustive description of the underlying bedload transport mechanism. In particular, this discrepancy highlights that the difference in the average waiting time is clearly underestimated, due to the fact that for the lowest transport condition, the convergence is not satisfied and the number of trajectory and waiting-time samples is not sufficient. The latter consideration is a straightforward consequence of the thick tails in the deep waiting time distribution, and should not be related to our data-acquisition strategy. In other words, longer measurements would still lead to an underestimation of the mean deep waiting times. Therefore, the truly key parameter resulting from this experimental study able to guide future transport models is not the average waiting time value but its power-law distribution (Table 3). Because the exponents seem to depend on the channel hydraulic conditions and wall shear stress, it is important to discuss their variability in a broader framework and compare them with estimated values from the literature.

As presented in Table 2 and discussed in section 2, the strict selection process required to identify waiting times unambiguously reduces the number of trajectories considerably. We quantified the selection-bias effect on the distribution of particle velocity, step time and step length by analyzing trajectories simply longer than $4D_{50}$. For the hydraulic conditions S4, increasing the number of trajectories from 261 to 2097, we observed a significant decrease in the averaged step time and step distance values (from 0.13 s to 0.08 s and from 8.2 mm to 4.5 mm, respectively), and a slight decrease in the mean particle velocity from 0.085 m s^{-1} to 0.078 m s^{-1}. However, the distributions were observed to exhibit consistent exponential tails for the three kinematic variables, for both data selections. We also verified that the choice of the velocity threshold defining the transition between motion and rest did not affect step length and step time statistics. Varying the threshold from 0.01 to 0.02 m s^{-1} led to less than 5% variation in the mean L_s and T_s values, for case S5, and negligible changes in the distributions. A possible explanation for the step-time invariance is that steps are defined in between resting times, which are less frequent at increasing transport rates, thus biasing our samples in the motion regime to short spatio-temporal extent.

5 Discussion

Three different experimental procedures have so far been used to quantify the distribution of particle resting times under varying transport conditions: (i) particle imaging methods [*Heyman et al*., 2013, *Martin et al.* 2014, *Cecchetto et al.* 2018], (ii) tracer-particle detection during high transport events [*Olinde and Johnson*, 2015] and (iii) bed-elevation measurements allowing for the reconstruction of resting times based on the time interval between local deposition and erosion events [*Voepel et al.* 2013, following *Wong et al.* 2007]. There seems to be an agreement that high transport rates, often associated with steep slopes, high Froude numbers, and bedform migrations are characterized by an exponential distribution of waiting times, shifting to a power-law distribution at progressively lower transport rates. The thinnest tails of the waiting time distribution were identified as an exponential decay function by *Heyman et al.* [2013] using the time interval between consecutive mass flux contributions. The transport regime was intense with supercritical

Froude number, antidune formation, and τ^*~0.1. *Martin et al.* [2014] used a narrow and short channel with a steep (6%) slope and provided Eulerian resting times using 2D imaging from the side. The tails of the exceedance probability were thick, with slope approximately -1, corresponding to a PDF power-law distribution with an exponent of -2. Such a value is consistent with the active-waiting-time distribution estimated here, but not as thick as the deep waiting time. *Martin et al.* [2014] used glass beads with uniform diameter, which likely reduced the ability of bed-surface heterogeneities to trap and shelter particles on the bed, thus reducing the probability of very long waiting times. *Cecchetto et al.* [2018] used an annular flume under low bedload transport, in a similar range as that investigated here, and observed consistent thick-tailed distributions of the waiting times, ranging from -1.3 to -1.0.

The effect of particle-size dispersion is accounted for in the field measurements by *Olinde & Johnson* [2015] based on the deployment and recovery of tracer particles during high sediment-transport events. *Olinde & Johnson* [2015] estimated an exceedance probability with a thick-tailed power-law distribution with exponents ranging from 0.24 to 0.72, with reported average of 0.67, corresponding to a PDF exponent b =-1.34, thus in line with the measurements provided here for the deep waiting times (-0.83 to -1.32). Another interesting comparison of our findings regarding the particle waiting time PDF can be made with the results found by *Voepel et al*. (2013) that analyzed the dataset of *Wong et al.* (2007). This dataset is made up of time series of bed fluctuations measured at different streamwise locations during flume experiments under equilibrium conditions in the absence of bedforms, with bedload transport of well sorted fine gravel (D_{50} ~ 7 mm) in near-critical conditions. In an Eulerian-based fashion, *Voepel et al.* (2013) analyzed these data and found the particle waiting time PDF under the hypothesis that (i) the time of particle deposition equates to the time that a fluctuating bed moves upwards and (ii) the time of particle entrainment equates to the time that a bed moves downwards. In more detail, they analyzed the run with $\tau^* = 0.117$ and by pooling together the time series of resting time computed at different bed elevations in the above-mentioned hypothesis, they estimated the empirical unconditional sediment-waiting-time distribution (i.e., the overall waiting time PDF) as a tempered Pareto distribution. The latter shows a power-law decay (heavy-tailed with infinite mean) up to a cutoff value, defined by a crossover time, depending on bed fluctuation and deposition depth; after that, the tail of the distribution becomes exponential (thus thinner and with finite mean).

For the case of the *Wong et al*. [2007] data, *Voepel et al.* [2013] found the exponent of the power law decay associated with resting time PDF equal to -1.72, in accordance with our results that exhibit a power-law decay with exponents ranging from -1.32 to -0.83 with a reasonable trend of decreasing exponents with increasing τ^* (from 0.029 to 0.042). In our experiments, the time of measurements is not long enough to observe a possible exponential tail but it is the first case that a Lagrangian-based experiment with coarse sand captures the power law decay of the waiting time PDF (at least up to a cutoff value). The power-law decay that fitted the waiting time PDF obtained in our experiments is also in agreement with the findings of *Nikora et al.* [2002], according to whom the intermediate stage of the motion may be characterized by both normal and anomalous diffusion (both super-diffusive and sub-diffusive), depending on what factors dominate. In our case, a sub-diffusive behavior may be hypothesized due to the thickness of the particle waiting time PDF and the exponential tail of the particle step length.

It is not simple to infer a general guideline to predict the waiting-time distribution from scattered experimental data in a variety of hydraulic and transport conditions and bed-material composition. However, we infer that in all the above experiments the waiting-time distribution appears to be controlled primarily by the grain-size heterogeneity and the sediment-transport rates. For low to moderate transport and non-perfectly homogeneous

sand-grain distributions, the waiting time PDF is predominantly observed as a power law, with power-law coefficient in the tails starting around -2 and approaching -1, toward critical mobility. Further in-depth analysis is required to understand this transition, as this experiment is not designed specifically to study the particle behavior at incipient sediment motion when a jamming transition occurs [*Ausillous* et al., 2016]. However, we may speculate that the particle transport intermittency [*Singh et al.*, 2009b; *Lee and Jerolmack*, 2018] and non-locality [*Pelosi and Parker*, 2014] that characterize the onset of motion are likely to be responsible for long resting times contributing to the heavy tails of the distribution [*Schumer et al*., 2009b] at low transport rates. For larger transport rates and steeper slopes, it is possible that the entire upper layer of the bed is mobilized, reducing the intermittency and the effects of grain-size heterogeneity. In that case, a Poissonian particle transport process can be assumed correctly and the waiting-time distribution shifts from thick to thin exponential tails, as observed by *Heyman* [2016]. In terms of future research efforts, it is still not clear how bedform formation and migration can change the waiting-time distribution, as well as the characteristics of the particle motion regime and their possible relation to rough wall turbulence scaling, as discussed here.

6 Conclusions

A series of experiments has been performed to study the kinematic properties of sediment particles of non-perfectly uniform size (D_{50} = 1.1mm, D_{20} = 0.9mm, D_{80} = 1.4mm) during bedload transport at conditions close to critical mobility. Particle trajectories have been captured by a slightly submerged camera, and the error in positioning has been quantified using the fluctuation in estimated particle size along the same trajectory. The investigated parameter space comprise 5 different conditions for u_*/u_{*c} in the range between 1.1 and 1.5, with the critical velocity value defined as the limiting case of no particle transported. Particular care was devoted to the classification of particle motion and resting regimes and to the associated statistical properties. The results of our experiments showed that particle streamwise and spanwise velocity components, as well as the step time and step length exhibit thin, exponential tails under all the investigated transport conditions; the acceleration also shows a thin-tailed Laplacian distribution (see, e.g., *Roseberry et al.* [2012] *Ancey and Heyman* [2014] and *Heyman et al.* [2014]).

Reasonable scaling quantities for normalization and modeling of particle kinematics variables in the motion regime are identified as the sediment diameter (length scale) and the shear velocity u_* (velocity scale). The Lagrangian evolution of particle velocity and acceleration, thus along a trajectory, shows, on average, a sharp increase when the particle starts moving, followed by a gentle, longer, decrease. Such temporal asymmetric behavior suggests a fast destabilizing effect from particle collisions or turbulent sweep motions, followed by a more persistent deceleration likely due to particle wall interactions or turbulent ejection events. The transition is marked by a switch in sign of the particle acceleration which occurs at a Lagrangian time $\tau u_*/D_{50}$ ~1–2, confirming the rough-wall frictional scaling proposed by *Campagnol et al.* (2015). The waiting times have been distinguished as *active* and *deep*. Active waiting time includes particles rocking back and forth, unable to find a stable position in the bed-sediment matrix. Active waiting time scales with the integral time scale of the turbulent flow near the wall, and can be approximated as ~ D_{50}/u_*. The deep waiting times, instead, point at particles unequivocally resting on the bed, and thus obeying a much longer and elusive time scale. Both the probabilistic distributions of the active and deep waiting times exhibit power-law tails, in particular near critical mobility conditions. A lack of convergence for the mean deep waiting time values is inferred, which implies that a larger spatio-temporal observation domain may still not be enough to quantify the waiting-time statistics unambiguously. The lack of convergence can be interpreted in terms of biased

estimates due to the combination of thick-tailed distributions and limitations in data acquisition, such as truncation (see *Ballio et al.* 2019). However, based on comparison with the literature, and in view of the observed trends between active and deep waiting times, increasing the wall shear stress, it is likely that the power-law tails may become less thick with increasing transport rates and with more uniform bed-material composition, approaching an exponential distribution. The reduction of tail thickness with increasing Shields parameter is also expected to reduce the bias of the waiting-time estimates. The overall mass flux contribution by bedload transport under the investigated conditions appears to be governed mostly by the particle velocity u_p, reasonably scaling with u_* (see Abbot and *Francis* [1977], *Nino et al.*[1994]), and by the waiting times. The particle step time is observed to remain fairly invariant, whereas the step length is mostly affected by u_p. The variability of u_p is quantified in terms of streamwise acceleration variance, which also depends on u_* and thus on the turbulent intensities.

In summary, we recognize that the particle episodic motion comprises two regimes: one is the motion or step regime, which is fairly well known, characterized by thin-tailed distributed variables, and interpretable with the phenomenology and the scaling of rough wall turbulence (in the absence of bedforms). The other one, the waiting or resting regime, is less tractable and more affected by measuring limitations due to the thick-tailed, power-law distributed, deep waiting times, which force average values to depend on the spatio-temporal domain of the experimental observations, under the near-critical mobility condition explored here. A very recent method was proposed by *Ballio et al.* [2019] to mitigate the effect of spatial and temporal censorship and to estimate unbiased averaged values for the step time, length and, especially, waiting times: those authors specifically addressed the case of power-law-distributed waiting times, suggesting that our statistics could be compensated and the shape of the distributions reassessed recursively in future analyses. The effect of varying transport conditions should still be addressed by more experimental and numerical works (see, e.g., *Gonzales et al.* [2017] and *Yager et al.* [2018]) on bedload transport to unambiguously unveil the transition from thick to thin tails in the waiting-time distribution. That information is critical to expand the more computationally effective stochastic modeling to particle transport and to understand the link between the waiting-time distribution and the sub-diffusive dispersion of particles in river beds inferred by *Fan* et al [2016].

Acknowledgments

This research has been supported by the National Natural Science Foundation of China (Grant No. 51909093 and Grant No. 41930643) providing financial help to the first author Mingxiao Liu. Mingxiao Liu also received a fellowship from the China Scholarship Council for her visit to the University of Minnesota. The (partial) financial support of NSF CAREER is gratefully acknowledged by Michele Guala, who values many discussions with Efi Foufoula-Georgiou, Arvind Singh, and Niannian Fan that led to this investigation. We are also grateful to our current and past reviewers, in particular Dr. Joris Heyman, Dr. Francesco Ballio and Dr. Zi Wu. Mingxiao Liu is grateful for the valuable help from Mirko Musa and Michael Heisel in experiments and other work. The data obtained during this laboratory investigation are included in the Supplemental Information and are thus available to the readers and the public through the journal website. We also uploaded 5 videos per transport condition, with a related table of hydraulic and sample geometry parameters, to the University of Minnesota data repository, which are available at https://conservancy.umn.edu/handle/11299/204778

References

Abbott, J., and J. Francis (1977), Saltation and suspension trajectories of solid grains in a water stream, *Philos. Trans. R. Soc. London*, Ser. A, 284, 225–254.

Ali SZ, Dey S. 2019 Bed particle saltation in turbulent wall-shear flow: a review. Proc. R. Soc. A 475: 20180824. http://dx.doi.org/10.1098/rspa.2018.0824L354

Abrahams, A. D. (2003), Bed-load transport equation for sheet flow, *J. Hydraul. Eng.-ASCE*, 129(2), 159–163, doi:10.1061/(ASCE)0733-9429(2003)129:2(159).

Abrahams, A. D., and P. Gao (2006), A bed-load transport model for rough turbulent open-channel flows on plane beds, *Earth Surf. Process. Landforms.*, 31(7), 910–928, doi:10.1002/esp.1300.

Ancey, C. (2010), Stochastic modeling in sediment dynamics: Exner equation for planar bed incipient bed load transport conditions, *J. Geophys. Res.*, 115, F00A11, doi:10.1029/2009JF001260.

Aussillous, P., Z. Zou, E. Guazzelli, L. Yan, L. and M. Wyart (2016) Scale-free channeling patterns near the onset of erosion of sheared granular beds. Proc. Natl. Acad. Sci. 113, 11788–11793.

Ancey, C., and J. Heyman (2014), A microstructural approach to bed load transport: Mean behaviour and fluctuations of particle transport rates, *J. Fluid Mech.*, 744, 129–168.

Ballio, F., Pokrajac, D., Radice, A., Hosseini Sadabadi, S. A. (2018), "Lagrangian and Eulerian description of bed load transport", Journal of Geophysical Research: Earth Surface, 123. doi: 10.1002/2016JF004087

Ballio, F., Radice, A., Fathel, S. L., & Furbish, D. J. (2019). "Experimental censorship of bed load particle motions and bias correction of the associated frequency distributions.", Journal of Geophysical Research: Earth Surface, 124, 116-136. doi: 10.1029/2018JF004710

Bagnold, R. A. (1966), An approach to the sediment transport problem from general physics, *U.S. Geol. Surv. Prof. Pap.*, 4221, 1–37.

Bagnold, R. A. (1973), The nature of saltation and of 'bed-load' transport in water, *Proc. R. Soc. London*, Ser. A, 332, 473–504.

Bagnold, R. A. (1977), Bed load transport by natural rivers, *Water Resour. Res.*, 13(2), 303–312.

Ball, A. E. (2012), Measurements of bed load particle diffusion at low transport rates, *Junior thesis*, Vanderbilt Univ., Nashville, Tenn.

Best, J. (2005), The fluid dynamics of river dunes: A review and some future research directions, *J. Geophys. Res.*, 110, F04S02F4, doi:10.1029/2004JF000218.

Bialik, R. J., V. I. Nikora, and P. M. Rowinski (2012), 3D Lagrangian modelling of saltating particles diffusion in turbulent water flow, *Acta Geo-phys.*, *60*(6), 1639–1660.

Bradley,D.N., G. E. Tucker, andD. A. Benson (2010), Fractional dispersion in a sand bed river, *J. Geophys. Res.*, 115, F00A09, doi:10.1029/2009JF001268.

Cao, Z.X., C.C. Xia, G. Pender, and Q.Q. Liu (2017), Shallow Water Hydro-Sediment-Morphodynamic Equations for Fluvial Processes, *J. Hydraul. Eng.-ASCE*, 2017, 143(5): 02517001, doi: 10.1061/(ASCE)HY.1943-7900.0001281

Campagnol J., Radice A., Nokes R., Bulankina V., Lescova A., Ballio F., (2013), "Lagrangian analysis of bed-load sediment motion: database contribution", Journal of Hydraulic Research, Vol. 51(5), 589-596. DOI: 10.1080/00221686.2013.812152.

Campagnol J., Radice A., Ballio F., and Nikora V. (2015), "Particle motion and diffusion at weak bed load: accounting for unsteadiness effects of entrainment and disentrainment", Journal of Hydraulic Research, vol. 53(5), 633-648. Doi: 10.1080/00221686.2015.1085920

Cecchetto, M., Tregnaghi, M., Bottacin-Busolin, A., Tait, S. J., Cotterle, L., & Marion, A. (2018). "Diffusive regimes of the motion of bed load particles in open channel flows at low transport stages.", Water Resources Research, 54. https://doi.org/10.1029/2018WR022885

Church, M. (2006), Bed material transport and the morphology of alluvial river channels, Annu. Rev. Earth Planet. Sci., 34, 325–354, doi:10.1146/annurev. earth.33.092203.122721.

Durán, O., B. Andreotti, and P. Claudin (2012), Numerical simulation of turbulent sediment transport, from bed load to saltation, *Phys. Fluids*, 24(10), 103306, doi:10.1063/1.47576 62.

Einstein, H. A. (1937), Der Geschiebetrieb als Wahrscheinlichkeitsproblem, in *Mitteilung der Versuchsanstalt für Wasserbau an der Eidgenössische Technische Hochschule Zürich*, Rascher, Zurich, Switzerland, English translation, Sedimentation, edited by H. W. Shen, pp. C1–C105, Colo. State Univ., Fort Collins.

Einstein, H. A. (1950), The Bed-Load Function for Sediment Transportation in Open Channel Flows, Technical Bulletin, vol. 1026, pp. 78, Soil Conserv. Serv., U.S. Dep. of Agric., Washington, D. C.

Ergenzinger, P. (1988), The nature of coarse material bed load transport, in Sediment Budgets: Proceedings of a Symposium Held at Porto Alegre, edited by M. P. Bordas, and D. E. Walling, IAHS Publ., 174, 207–216.

Escauriaza, C., and F. Sotiropoulos (2009), Trapping and sedimentation of inertial particles in three‐dimensional flows in a cylindrical container with exactly counter‐rotating lids, J. Fluid Mech., 641, 169–193.

Escauriaza, C., and F. Sotiropoulos (2011), Lagrangian model of bed‐load transport in turbulent junction flows, J. Fluid Mech., 666, 36–76.

Fan, N., D. Zhong, B. Wu, E. Foufoula-Georgiou, and M. Guala (2014), A mechanistic-stochastic formulation of bed load particle motions: From individual particle forces to the Fokker-Planck equation under low transport rates, *J. Geophys. Res.* Earth Surf., 119, 464–482, doi: 10.1002/2013JF002823.

Fan, N., A. Singh, M. Guala, E. Foufoula-Georgiou, and B. Wu (2016), Exploring a semimechanistic episodic Langevin model for bed load transport: Emergence of normal and anomalous advection and diffusion regimes, *J. Geophys. Res.* Earth Surf., 52(4), 2789–2801, doi: 10.1002/2015WR018023.

Furbish, D. J., J. C. Roseberry, and M. W. Schmeeckle (2012a), A probabilistic description of the bed load sediment flux: 3. The particle velocity distribution and the diffusive flux, *J. Geophys. Res.*, 117, F03033, doi:10.1029/2012JF002355.

Furbish, D. J., P. K. Haff, J. C. Roseberry, and M. W. Schmeeckle (2012b), A probabilistic description of the bed load sediment flux: 1. Theory, *J. Geophys. Res.*, 117, F03031, doi:10.1029/2012JF002352.

Furbish, D. J., A. E. Ball, and M. W. Schmeeckle (2012c), A probabilistic description of the bed load sediment flux: 4. Fickian diffusion at low transport rates, *J. Geophys. Res.*, 117, F03034, doi:10.1029/2012JF002356.

Furbish, D. J., and M. W. Schmeeckle (2013), A probabilistic derivation of the exponential-like distribution of bed load particle velocities, *Water Resour. Res.*, 49, 1537–1551, doi:10.1002/wrcr.20074.

Frey, P., and M. Church (2011), Bedload: A granular phenomenon, *Earth Surf. Process. Landforms.*, *36*(1), 58–69.

Ganti, V., M. Meerschaert, E. Foufoula‐Georgiou, E. Viparelli, and G. Parker (2010), Normal and anomalous diffusion of gravel tracer particles in rivers, *J. Geophys. Res.*, 115, F00A12, doi:10.1029/2008JF001222.

González C., D.H. Richter, D. Bolster, S. Bateman, J. Calantoni, and C. Escauriaza (2017). Characterization of bedload intermittency near the threshold of motion using a Lagrangian sediment transport model, *Environ. Fluid Mech.*, 17 (1), 111-137

Guillaume, P. and R. Alain (2017), Effects of check dams on bed-load transport and steep-slope stream morphodynamics, *Geomorphology*, 291, 94-105, doi:10.1016/j.geomorph.2016. 03.001.

Habersack, H. M. (2001), Radio-tracking gravel particles in a large braided river in New Zealand: A field test of the stochastic theory of bed load transport proposed by Einstein, Hydrol. Processes, 15(3), 377–391.

Han, Q. W., and M. M. He (1980), *Stochastic models for bed load particle diffusion and the statistical properties* [in Chinese], Sci. China, 4, 396–401.

Heyman, J., Ma, H. B., Mettra, F. & Ancey, C. Spatial correlations in bed load transport: Evidence, importance, and modelling. Journal of Geophysical Research: Earth Surface, 119, 1751-1767, doi:10.1002/2013jf003003 (2014).

Heyman, J., Ma, H. B., Mettra, F. & Ancey, C. Statistics of bedload transport over steep slopes: Separation of time scales and collective motion. Geophysical Research Letters, 40(1), 128-133, doi:10.1029/2012GL054280 (2013)

Heyman J, Bohorquez P, Ancey C (2016) Entrainment, motion, and deposition of coarse particles transported by water over a sloping mobile bed. Journal of Geophysical Research: Earth Surface 121 (10), 1931-1952

Houssais, M. and E. Lajeunesse (2012), Bedload transport of a bimodal sediment bed, *J. Geophys. Res.*, 117, F04015, doi:10.1029/2012JF002490, 2012.

Lajeunesse, E., L. Malverti, and F. Charru (2010), Bed load transport in turbulent flow at the grain scale: Experiments and modeling, *J. Geophys. Res.*, 115, F04001, doi:10.1029/2009JF001628.

Lee, D. B., and D. Jerolmack (2018), Determining the scales of collective entrainment in collision-driven bed load, Earth Surf. Dynam., 6, 1089–1099. doi: 10.5194/esurf-6-1089-2018

Liu, Y., F. Metivier, E. Lajeunesse, P. Lancien, C. Narteau, and P. Meunier (2008), Measuring bed load in gravel-bed mountain rivers: Averaging methods and sampling strategies, *Geodin. Acta*, 21, 81–92.

Martin, R. L., D. J. Jerolmack, and R. Schumer (2012), The physical basis for anomalous diffusion in bed load transport, *J. Geophys. Res.*, 117, F01018, doi:10.1029/2011JF00 2075.

Martin, R. L., P. K. Purohit, and D. J. Jerolmack (2014), Sedimentary bed evolution as a mean-reverting random walk: Implications for tracer statistics, *Geophys. Res. Lett.*, 41, 6152–6159, doi:10.1002/2014GL060525.

Métivier, F., P.Meunier,M.Moreira, A. Crave, C. Chaduteau, B. Ye, and G. Liu (2004), Transport dynamics andmorphology of a highmountain stream during the peak flow season: The Ürümqi River (Chinese Tian Shan), in *River Flow* 2004, vol. 1, pp. 770–777, A. A. Balkema, Leiden, Netherlands.

Meunier, P., F. Métivier, E. Lajeunesse, A. S. Meriaux, and J. Faure (2006), Flow pattern and sediment transport in a braided river: The “torrent de St Pierre” (French Alps), *J. Hydrol.*, 330, 496–505.

Mo, J., and M.G. Raizen, Highly Resolved Brownian Motion in Space and in Time, Annual Review of Fluid Mechanics, 51, 401-428, 2019.

Nikora, V., H. Habersack, T. Huber, and I. McEwan (2002), On bed particle diffusion in gravel bed flows under weak bed load transport, *Water Resour. Res.*, 38(6), 1081, doi:10.1029/2001WR000513.

Niño, Y. and M.H. Garcia(1996), Experiments on particle-turbulence interactions in the near-wall region of an open channel flow: implications for sediment transport, *J. Fluid Mech.*, 326, 285-319.

Niño, Y., and M. García (1998a), Experiments on saltation of sand in water, *J. Hydraul. Eng.-ASCE*, 124(10), 1014–1025.

Niño, Y., and M. García (1998b), Using Lagrangian particle saltation observations for bedload sediment transport modelling, *Hydrol. Process.*, 12(8), 1197–1218.

Niño Y, García M, Ayala L. 1994 Gravel saltation: 1 Experiments. Water Resour. Res. 30, 1907–1914. doi:10.1029/94WR00533

Olinde, L. & Johnson, J. P. L. Using RFID and accelerometer-embedded tracers to measure probabilities of bed load transport, step lengths, and rest times in a mountain stream. Water Resources Research 51, 7572-7589, doi:10.1002/2014wr016120 (2015).

Papanicolaou, A. N., P. Diplas, N. Evaggelopoulos, and S. Fotopoulos (2002), Stochastic incipient motion criterion for spheres under various bed packing conditions, J. Hydraul. Eng.-ASCE, 128(4), 369-380, doi: 10.1061/(ASCE)0733-9429(2002)128:4(369).

Pelosi, A., and G. Parker (2014), Morphodynamics of river bed variation with variable bedload step length, Earth Surf. Dynam., 2, 243–253. doi: 10.5194/esurf-2-243-2014

Pelosi, A., G. Parker, R. Schumer and H. B. Ma (2014), Exner-Based Master Equation for transport and dispersion of river pebble tracers: Derivation, asymptotic forms, and quantification of nonlocal vertical dispersion, *J. Geophys. Res. Earth Surf.*, *119*, 1818–1832, doi:10.1002/2014JF003130.

Pelosi, A., R. Schumer, G. Parker, and R. I. Ferguson (2016), The cause of advective slowdown of tracer pebbles in rivers: Implementation of Exner-Based Master Equation for coevolving streamwise and vertical dispersion, *J. Geophys. Res Earth Surf.*, 121, 623–637, doi:10.1002/2015JF003497.

Phillips, C. B., R. L. Martin, and D. J. Jerolmack (2013), Impulse framework for unsteady flows reveals superdiffusive bed load transport, *Geophys. Res. Lett*, 40, 1328–1333, doi:10.1002/grl.50323.

Rashidi, M., G. Hetsroni, and S. Banerjee. (1990) Particle-turbulence interaction in a boundary layer. *Intl J. Multiphase Flow.* 16, 935-949.

Roseberry, J. C., M. W. Schmeeckle, and D. J. Furbish (2012), A probabilistic description of the bed load sediment flux: 2. Particle activity and motions, *J. Geophys. Res.*, 117, F03032, doi:10.1029/2012JF002353.

Sayre, W., and D. Hubbell (1965), Transport and dispersion of labeled bed material, North Loup River, Nebraska, *U.S. Geol. Surv. Prof. Pap.*, 433-C, 48 pp.

Schmeeckle, M. W., and J. M. Nelson (2003), Direct numerical simulation of bedload transport using a local, dynamic boundary condition. *Sedimentology*, *50*(2), 279-301. doi: 10.1046/j.1365-3091.2003.00555.x.

Schmeeckle, M.W. (2014), Numerical simulation of turbulence and sediment transport of medium sand, *J. Geophys. Res. Earth Surf.*, 119(6), 1240-1262, doi: 10.1002/2013JF00 2911.

Schmidt, K. H., and P. Ergenzinger (1992), Bedload entrainment, travel lengths, step lengths, rest periods—Studied with passive (iron, magnetic) and active (radio) tracer techniques, *Earth Surf. Process. Landforms.*, 17(2), 147–165.

Schumer, R., and D. Jerolmack (2009), Real and apparent changes in sediment deposition rates through time, *J. Geophys. Res.*, 114, F00A06, doi:10.1002/esp.3290170204.

Schumer, R., Meerschaert, M. M. & Baeumer, B. (2009b).Fractional advection-dispersion equations for modeling transport at the Earth surface. Journal of Geophysical Research-Earth Surface 114, doi:10.1029/2008jf001246

Singh, A., S. Lanzoni, and E. Foufoula-Georgiou (2009), Nonlinearity and complexity in gravel bed dynamics, *Stoch. Env. Res. Risk A.*, 23(7), 967–975, doi:10.1007/s00477-008-0269-8.

Singh, A., E. Foufoula Georgiou, F. Porté Agel, P. R. Wilcock (2012), Coupled dynamics of the evolution of gravel bed topography, flow turbulence and sediment transport in an experimental channel. *J. Geophys. Res. Earth Surf.*, 117, F04016, doi:10.1029/2011JF002323.

Singh, A., K. Fienberg, D. J. Jerolmack, J. Marr, and E. Foufoula-Georgiou (2009), Experimental evidence for statistical scaling and intermittency in sediment transport rates, J. Geophys. Res., 114, F01025, doi:10.1029/2007JF000963.

Sumer, B. M., and B. Oguz, (1978) Particle motions near the bottom in turbulent flow in an open channel. *J. Fluid Mech.* 86, 109-127.

Sun, H.G., D. Chen, Y. Zhang, and L. Chen (2015), Understanding partial bed-load transport: Experiments and stochastic model analysis, *Journal of Hydrology*, 521, 196-204. doi:10. 1016/j.jhydrol.2014.11.064.

Tardu, S.F. (2002). Characteristics of single and multiple bursting events in the inner layer. Part 2. Level-crossing events. *Experiments in Fluids*, 33 (2002), 640–652, doi: 10.1007/ s00348-002-0482-z.

Voepel, H., R. Schumer, and M. A. Hassan (2013), Sediment residence time distributions: Theory and application from bed elevation measurements, *J. Geophys. Res. Earth Surf.*, 118, doi:10.1002/jgrf.20151.

Weeks, E. R., Urbach, J. S. & Swinney, H. L. Anomalous diffusion in asymmetric random walks with a quasi-geostrophic flow example. Physica D-Nonlinear Phenomena 97, 291-310, doi:10.1016/0167-2789(96)00082-6 (1996).

Wong, M., Parker, G., DeVries, P., Brown, T. M. & Burges, S. J. Experiments on dispersion of tracer stones under lower-regime plane-bed equilibrium bed load transport. Water Resources Research 43, W03440 (2007).

Wu, F. C., and K. H. Yang (2004), A stochastic partial transport model for mixed-size sediment: Application to assessment of fractional mobility, *Water Resour. Res.*, 40, W045014, doi:10.1029/2003WR002256.

Wu, Z., Foufoula-Georgiou, E., Parker, G., Singh, A., Fu, X., & Wang, G. (2019). Analytical solution for anomalous diffusion of bedload tracers gradually undergoing burial. Journal of Geophysical Research: Earth Surface, 124, 21–37. https://doi.org/10.1029/2018JF004654

Yager E.M. Schmeeckle M.W. and Boadoux A. (2018) Resistance is not futile: grain sresistance controls on observed critical Shields Stress variation. *J. Geophys. Res. Earth Surf.*, 123(12), doi.org/10.1029/2018JF004817

Yang, C. T., and W. W. Sayre (1971), Stochastic model for sand dispersion, *J. Hydraul. Div. Am. Soc. Civ. Eng.*, 97, 265–288.

Yalin, M. (1977), *Mechanics of Sediment Transport*, Pergamon, New York.

Zhang, Y., R. L. Martin, D. Chen, B. Baeumer, H. Sun and L. Chen (2014), A subordinated advection model for uniform bed load transport from local to regional scales, *J. Geophys. Res.* Earth Surf., 119, 2711–2729, doi:10.1002/2014JF003145.

Table 1: Hydraulic flow conditions: $U_{1.5}$ is the average flow velocity at z= 1.5cm above the bed, h is the flow depth, u_* is the shear velocity, $\tau = \rho u_*^2$ is the bed shear stress, θ is the Shields number, *Fr* and *Re* are the Froude and Reynolds numbers

Series	$U_{1.5}$ (m/s)	h (m)	u_* (m/s)	*Re*	*Fr*	τ (Pa)	θ
S1	0.33	0.157	0.018	39559	0.277	0.333	0.021
S2	0.34	0.169	0.022	43110	0.279	0.467	0.029
S3	0.35	0.172	0.023	44828	0.280	0.514	0.032
S4	0.37	0.177	0.024	48685	0.294	0.565	0.035
S5	0.38	0.179	0.026	50331	0.300	0.672	0.042

Table 2: Image recording parameters and particle tracking statistics

Series	Sampling window size (mm*mm)	sampling interval (sec)	N_{raw}	N_{gt}	N_s	Unique spatial coordinates of N_s	Duration (sec)
S1	80*60	0.0083	14220	678	261	20684	32*20
S2	63*48	0.0083	65777	3765	416	36388	32*20
S3	63*48	0.0083	68220	3962	400	22155	25*20
S4	71*53	0.0083	131659	8084	781	35271	34*20
S5	73*55	0.0083	160936	13792	1208	55387	24*20

Table 3. Particle transport average statistics < • > under varying shear velocity u_* in S1-S5 hydraulic conditions. $U_{1.5}$ is the streamwise flow velocity at z=1.5cm above the bed. T_{wa} and T_{wd} are the two definitions of waiting time (active and deep, respectively, as described in Chapter 3.3). T_s is the step time. L_s is the step distance. u_p is the streamwise velocity component of particle. std (a_s) is the standard deviation of the streamwise acceleration component of the particle. b indicates the exponents of the active and passive waiting time power-law distribution defined in Equation (3).

Series	u_* **(m/s)**	$< U_{1.5} >$ **(m/s)**	$< T_{wa} >$ **(s)**	$< T_s >$ **(s)**	$< L_s >$ **(mm)**	$< u_p >$ **(m/s)**	std (a_s) **(m/s^2)**	$< T_{wd} >$ **(s)**	b_{active}	$b_{passive}$
S1	0.018	0.327	0.24	0.08	3.45	0.050	4.38	-	-	-
S2	0.022	0.372	0.21	0.13	6.96	0.067	4.44	4.07	-1.55,	-0.83
S3	0.023	0.372	0.19	0.12	7.70	0.079	5.24	3.54	-1.33	-1.09
S4	0.024	0.377	0.17	0.13	8.17	0.085	5.38	3.98	-1.69	-1.13
S5	0.026	0.397	0.15	0.13	8.85	0.086	6.05	3.51	-1.94	-1.32

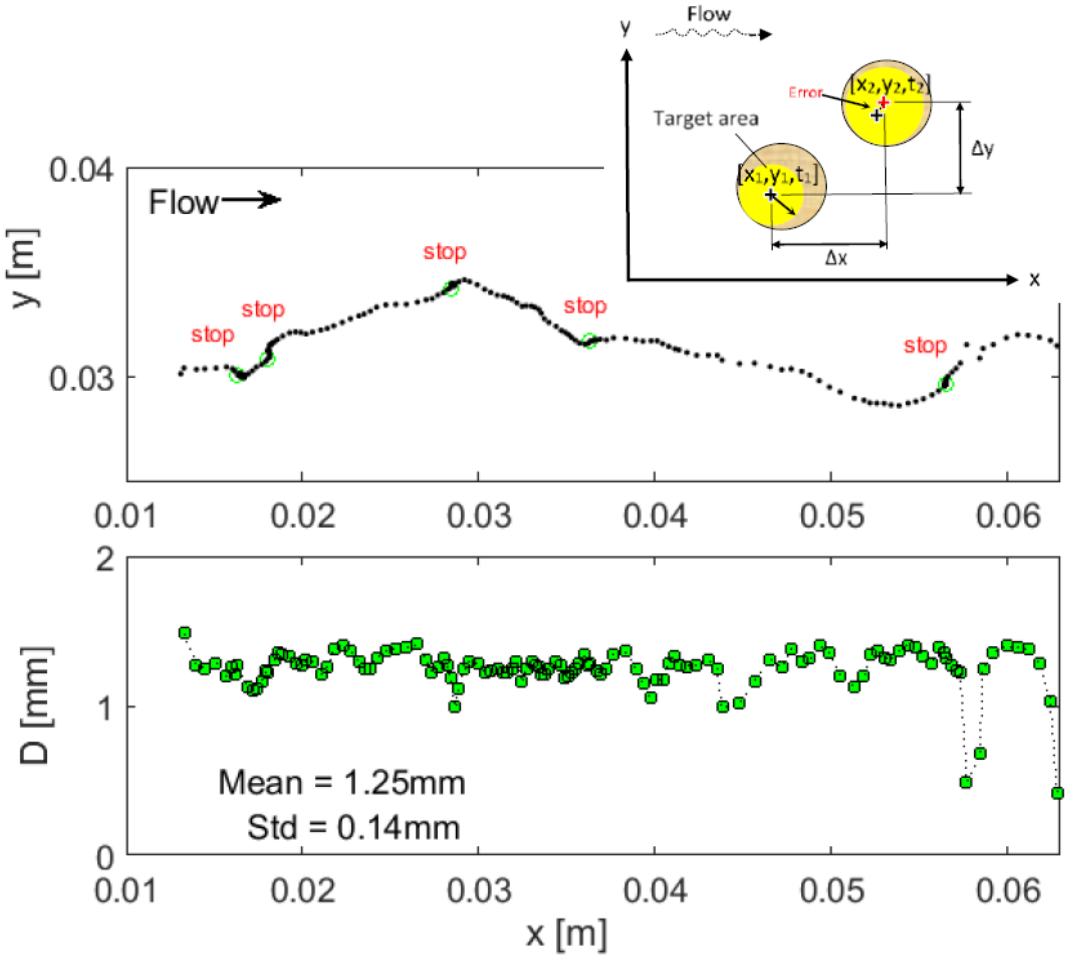

Figure 1. a) Particle trajectory in the streamwise-spanwise (x,y) spatial coordinates; b) variability of the particle equivalent diameter along the particle trajectory during motion and resting regimes (used here as a measure of experimental uncertainty) .

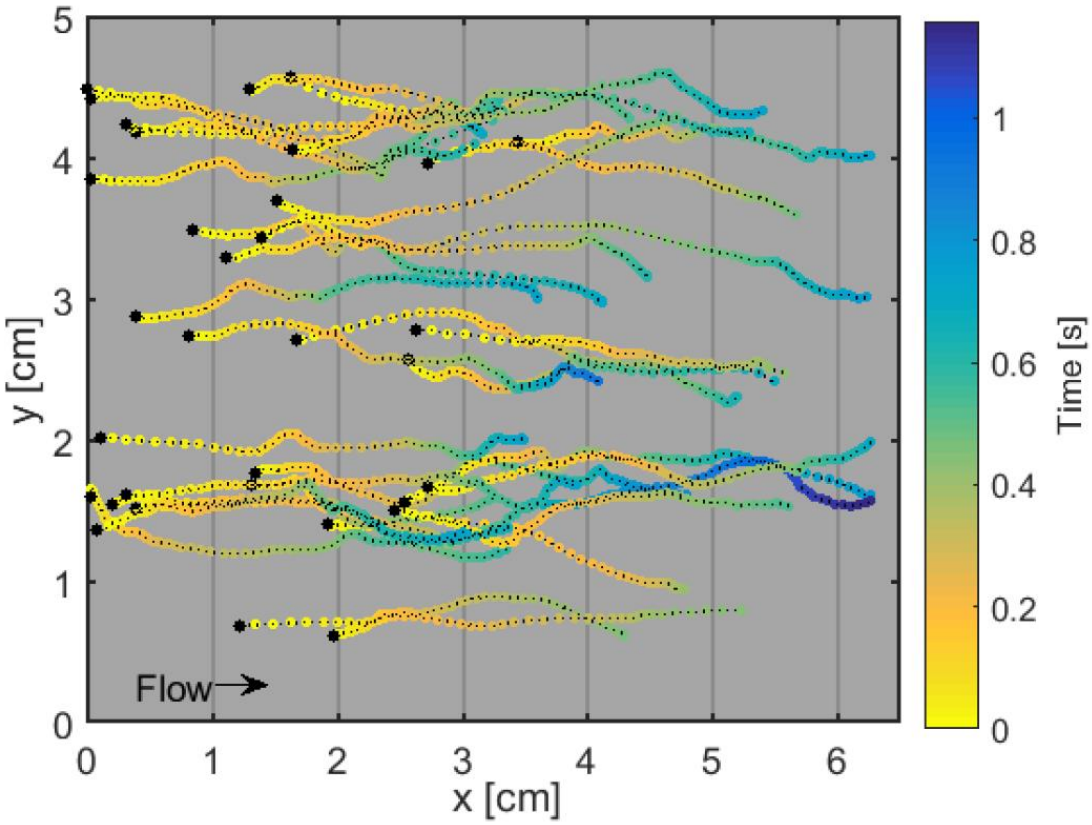

Figure 2. Tracked particles moving on the bed surface (Experiment S2). Time is reported in color coding with respect to the start of the video recording. Black circle denotes the first particle location detected.

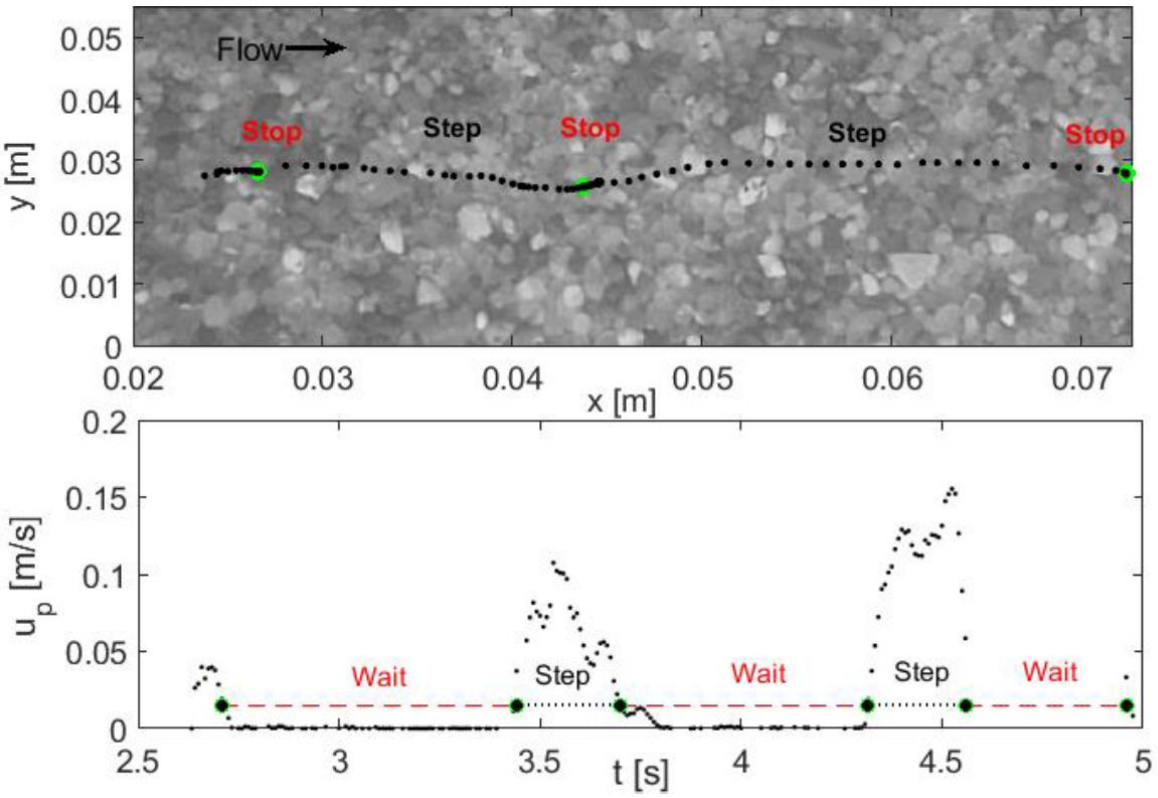

Figure 3. a) Particle trajectory on the [x,y] bed surface; b) Streamwise velocity component of the same trajectory plotted in time, allowing for the identification of the steps time T_s and length L_s (or hops) and the waiting (or rest) times T_w.

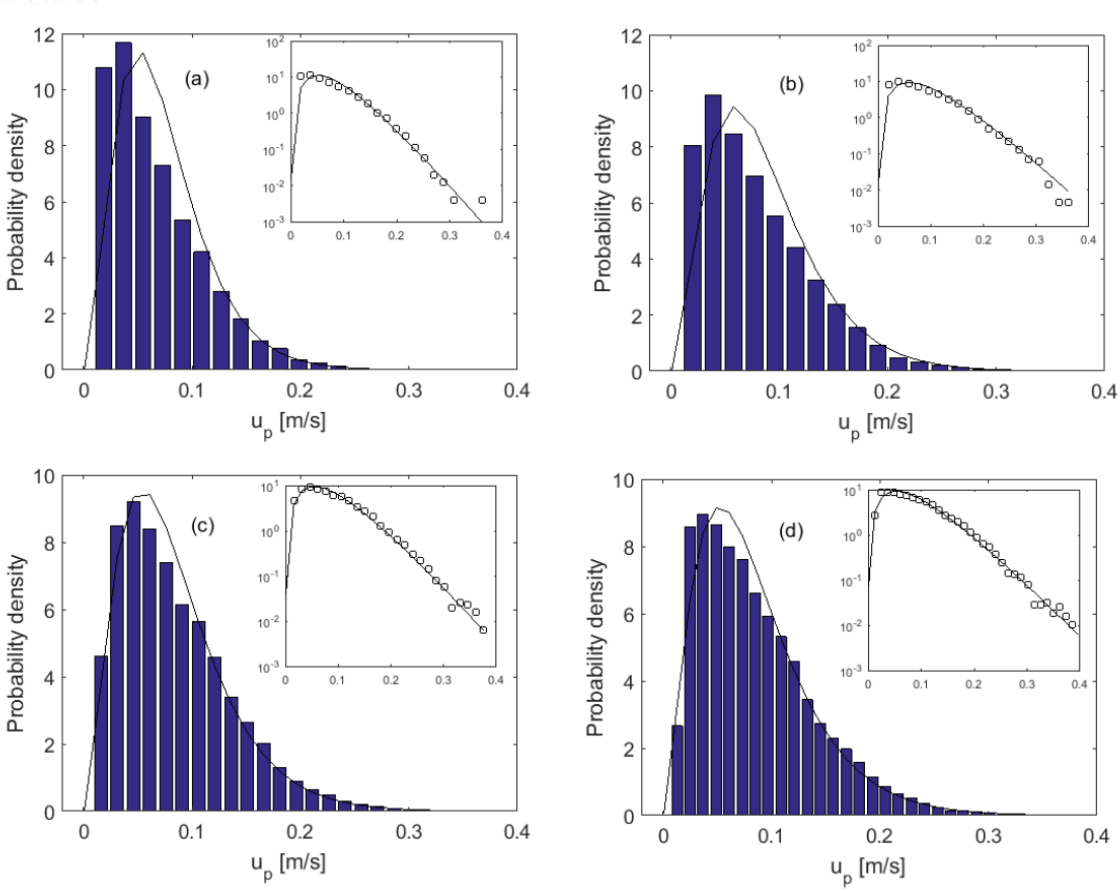

Figure 4. Distribution of the streamwise particle velocity component u_p for the four experimental conditions S2 to S5 in panels (a) to (d). The PDF is reported in semilog scale in all the insets. The parameters of the four distributions, referring to Equation (1), are (a, b) = (3.244, 0.022), (3.055, 0.028), (2.827, 0.030), and (2.618, 0.033).

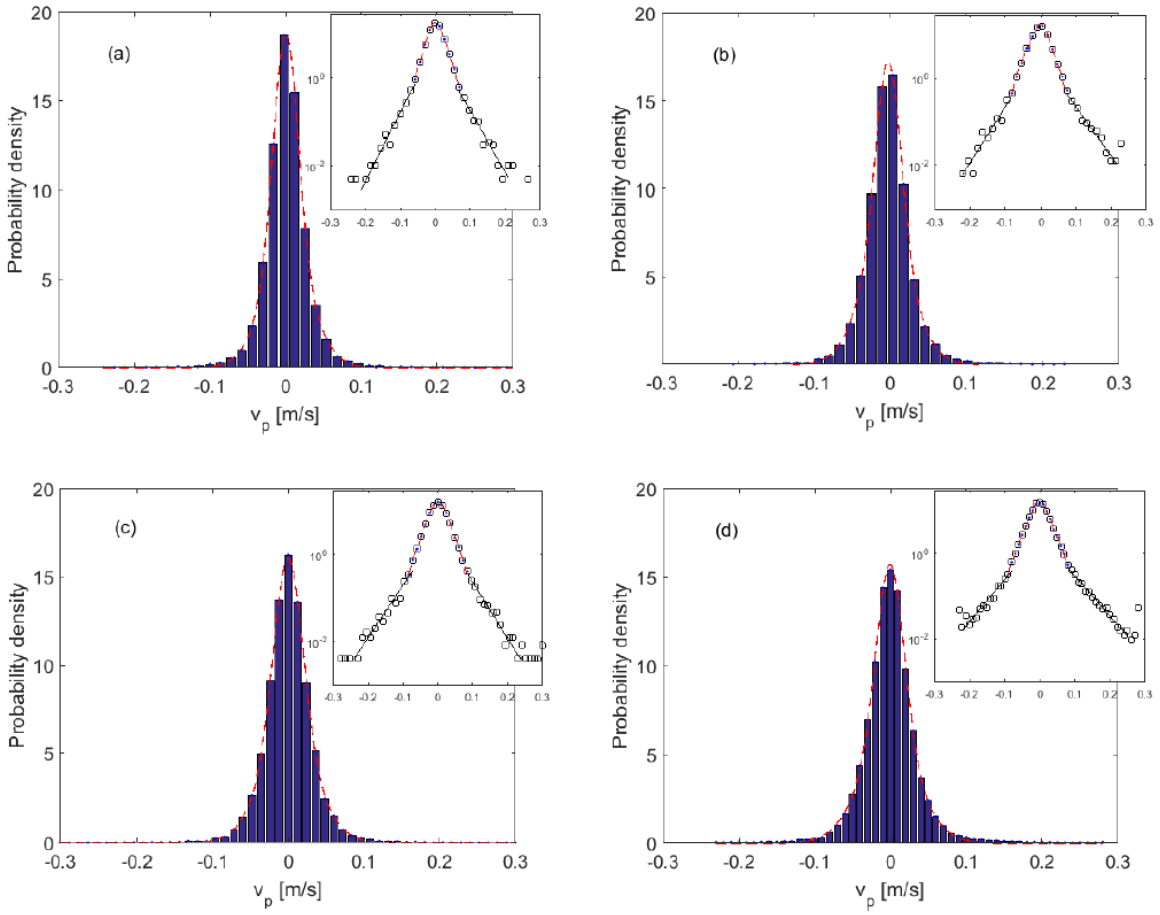

Figure 5. Distribution of the spanwise particle velocity component v_p for the four experiment conditions S2 to S5 in panels (a) to (d). The PDF is reported in semilog scale in all the insets. Two functions were used to fit the data: the red dashed line denotes the Gaussian fit whereas the black solid line denotes an exponential fit. The Standard deviations, std (v_p), are 0.029, 0.032, 0.033, and 0.038, respectively.

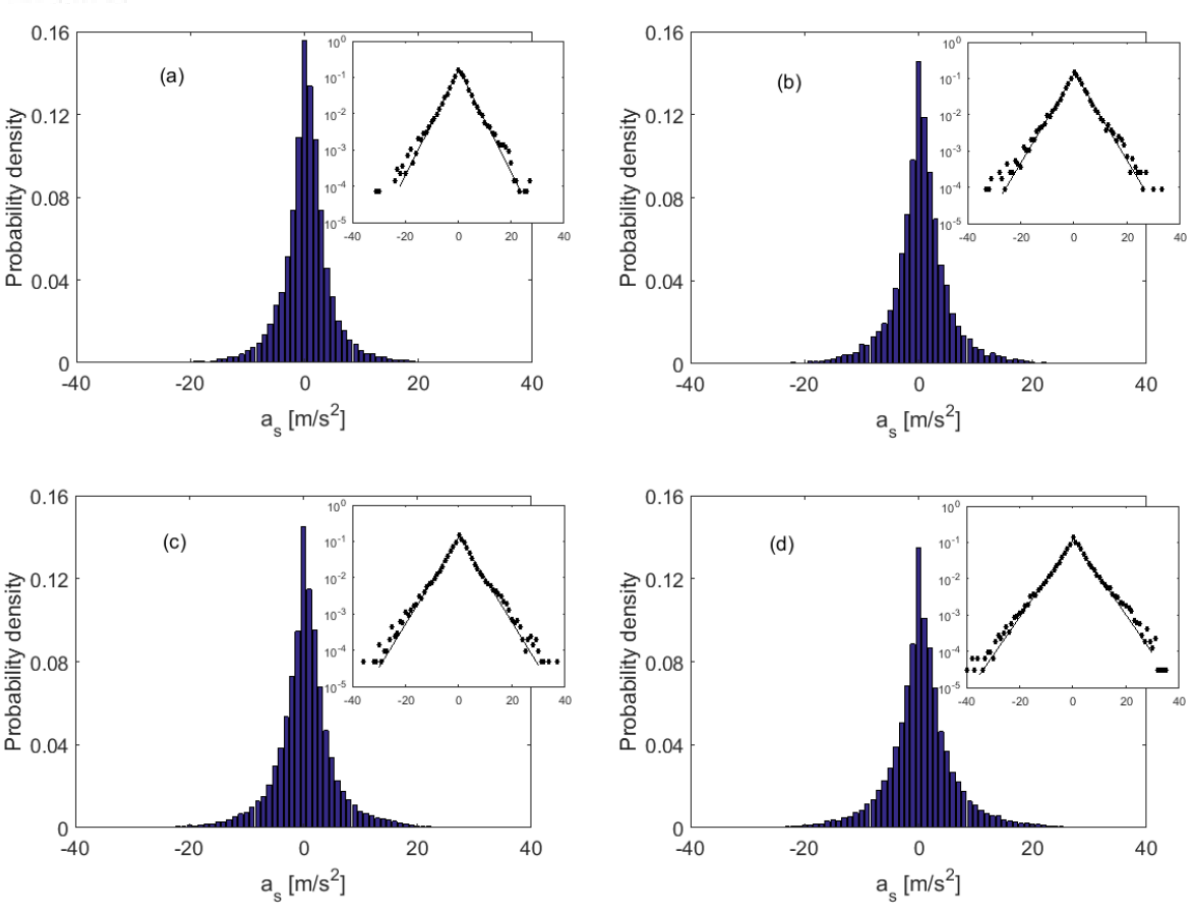

Figure 6. Distribution of the streamwise particle acceleration component a_s for the four experiment conditions S2 to S5 in panels (a) to (d). The PDF is reported in semilog scale in all the insets. The standard deviation of a_s is 4.4, 5.2, 5.4, and 6.1 m s^{-2} for cases S2 to S5. The parameters of the four distributions, referring to Equation (2), are (μ, b) = (0.33, 3.02), (0.30, 3.55), (0.23, 3.63), and (0.28, 4.10).

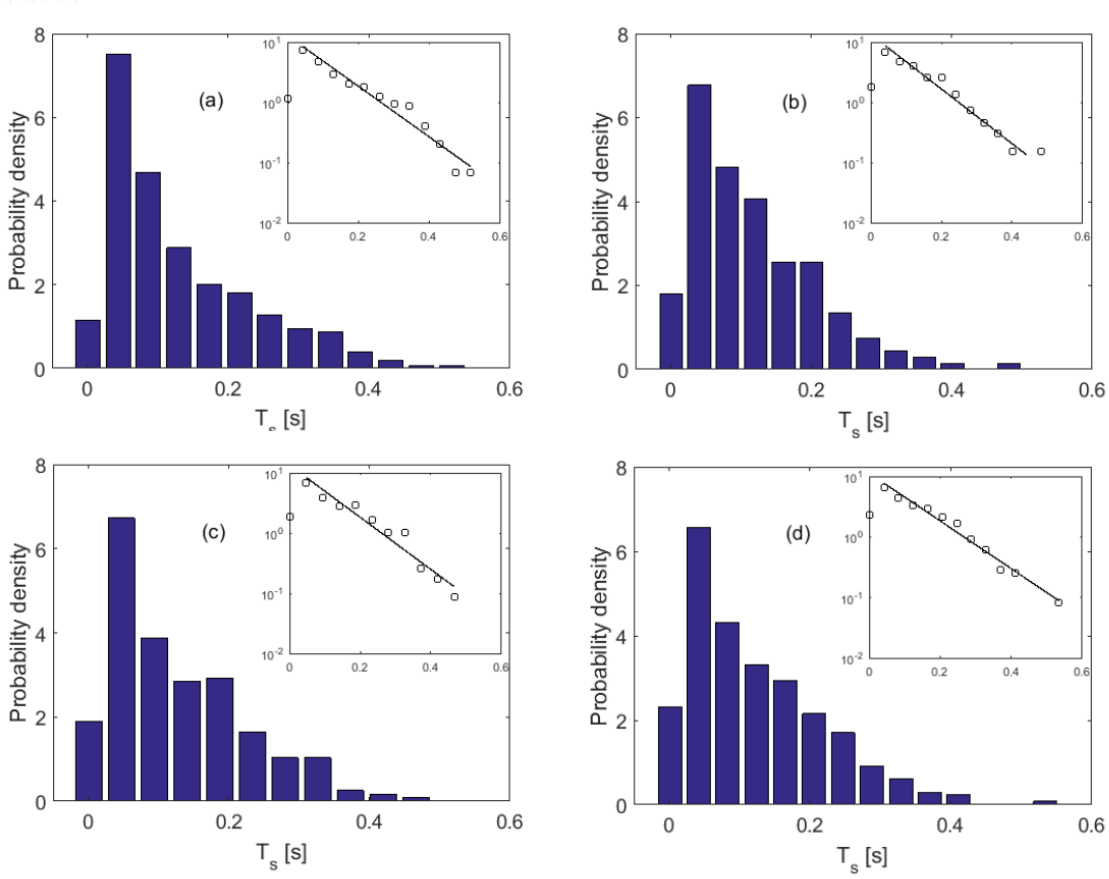

Figure 7. Distribution of the particle step time T_s for the four experimental conditions S2 to S5 in panels (a) to (d). The PDF is reported in semilog scale in all the insets. The mean value of the four experimental conditions is: $<T_s>$ =0.13, 0.12, 0.13, 0.13 s. The exponent of the PDF parameter is $-1/<T_s>$.

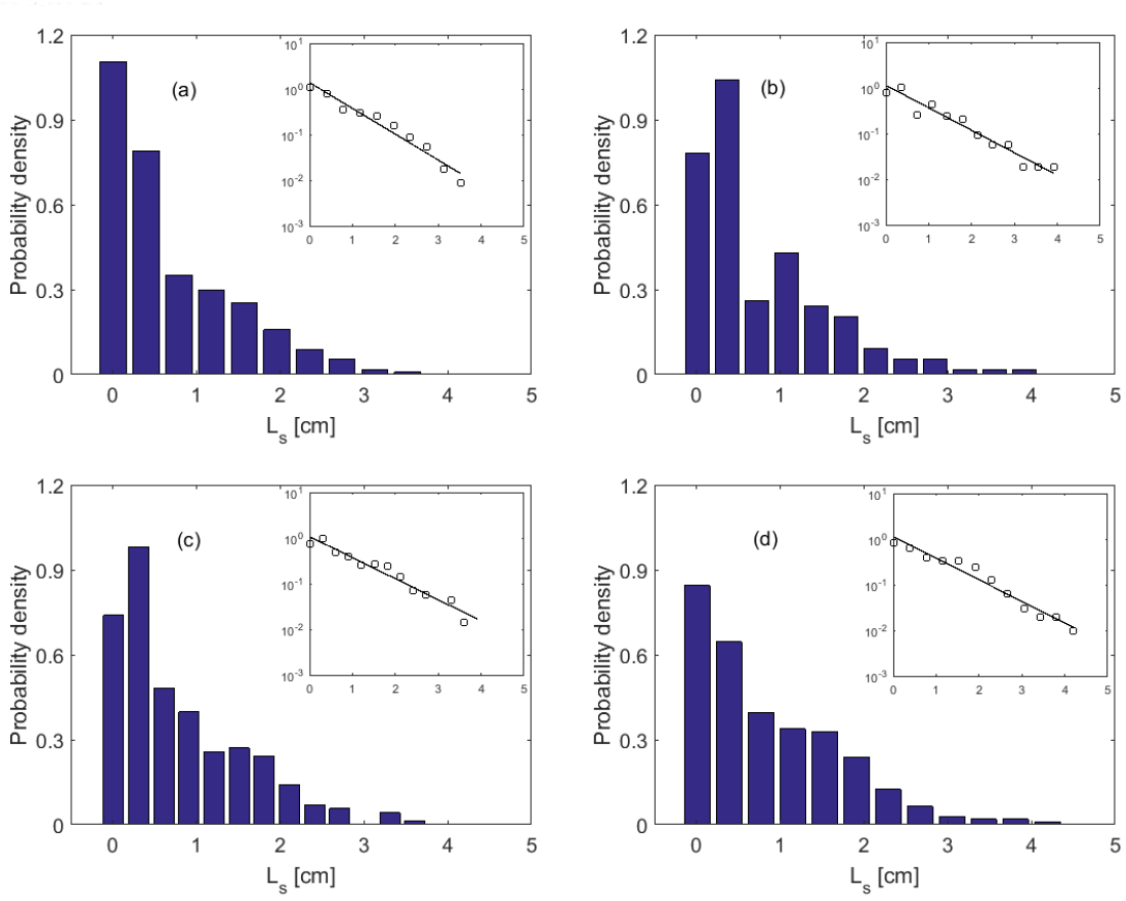

Figure 8. Distribution of the particle step length L_s for the four experimental conditions S2 to S5 in panels (a) to (d). The PDF is reported in semilog scale in all the insets. $\langle L_s \rangle$=0.70, 0.77, 0.82, 0.89 cm. The exponent of the PDF parameter is $-1/\langle L_s \rangle$.

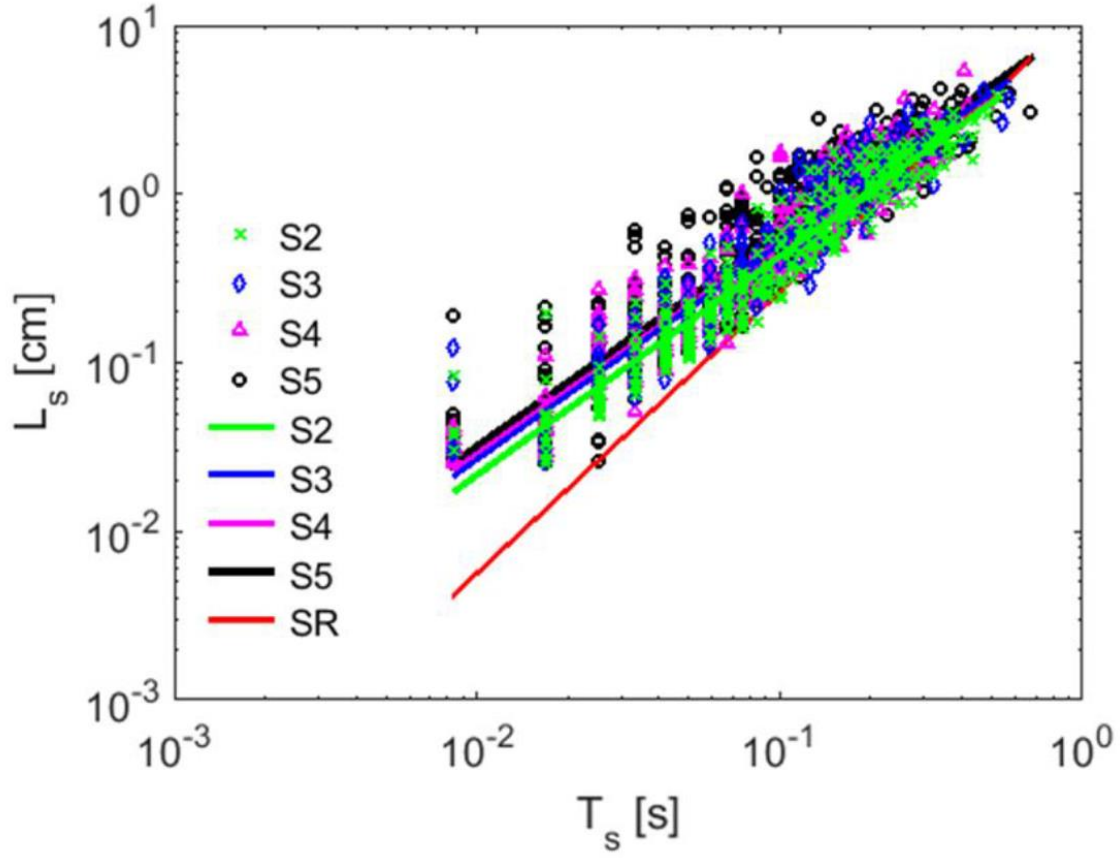

Figure 9. Joint scatter plot of the particle step time T_s and step length L_s for the four experimental conditions S2 to S5. The power law exponents were estimated as 1.30, 1.28, 1.26 and 1.26 with R2=0.92, 0.88, 0.89, 0.87 (S2–S5), respectively, compared with SR=5/3~1.67 (the slope of the experiment of *Roseberry et al.*, [2012]).

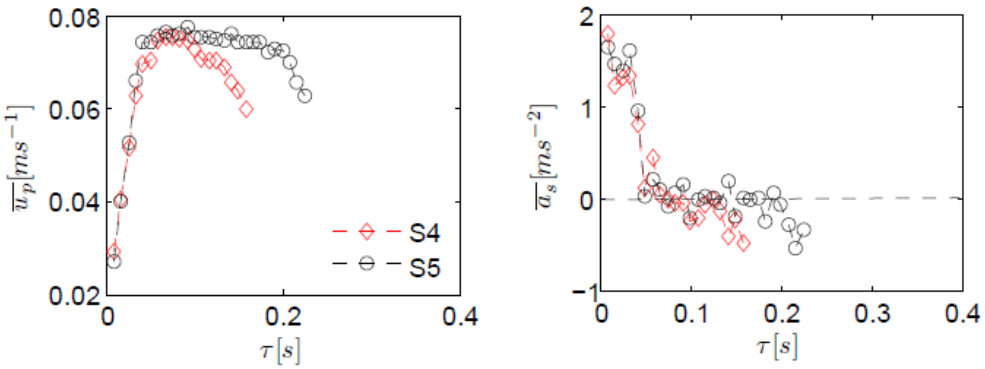

Figure 10. Conditional average of streamwise velocities u_p (a) and acceleration a_s (b) along particle trajectories as a function of the Lagrangian time τ, from experimental cases S4 and S5. To avoid sampling bias both datasets were obtained by averaging 60 trajectories of particles in motion for at least the largest time τ explored here.

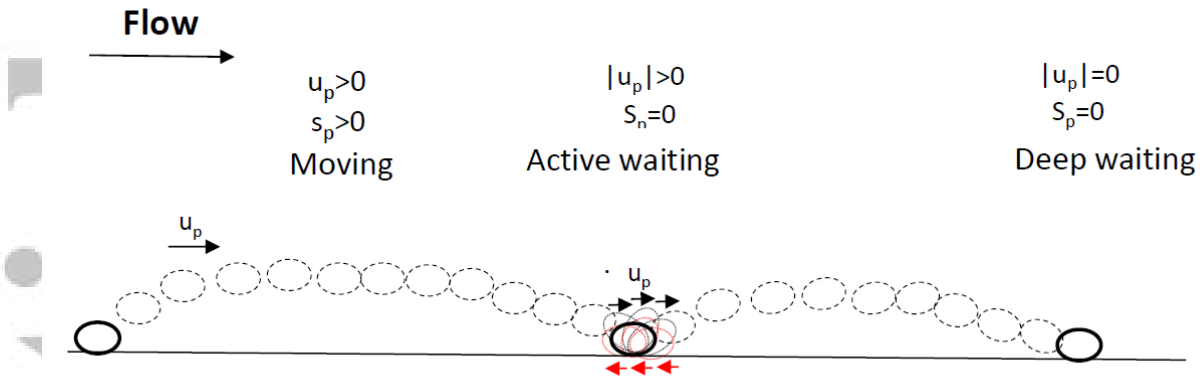

Figure 11. Schematic representation of the active and deep waiting time. u_p is the stream wise velocity of particles, and s_p is the net displacement of the particle centroid.

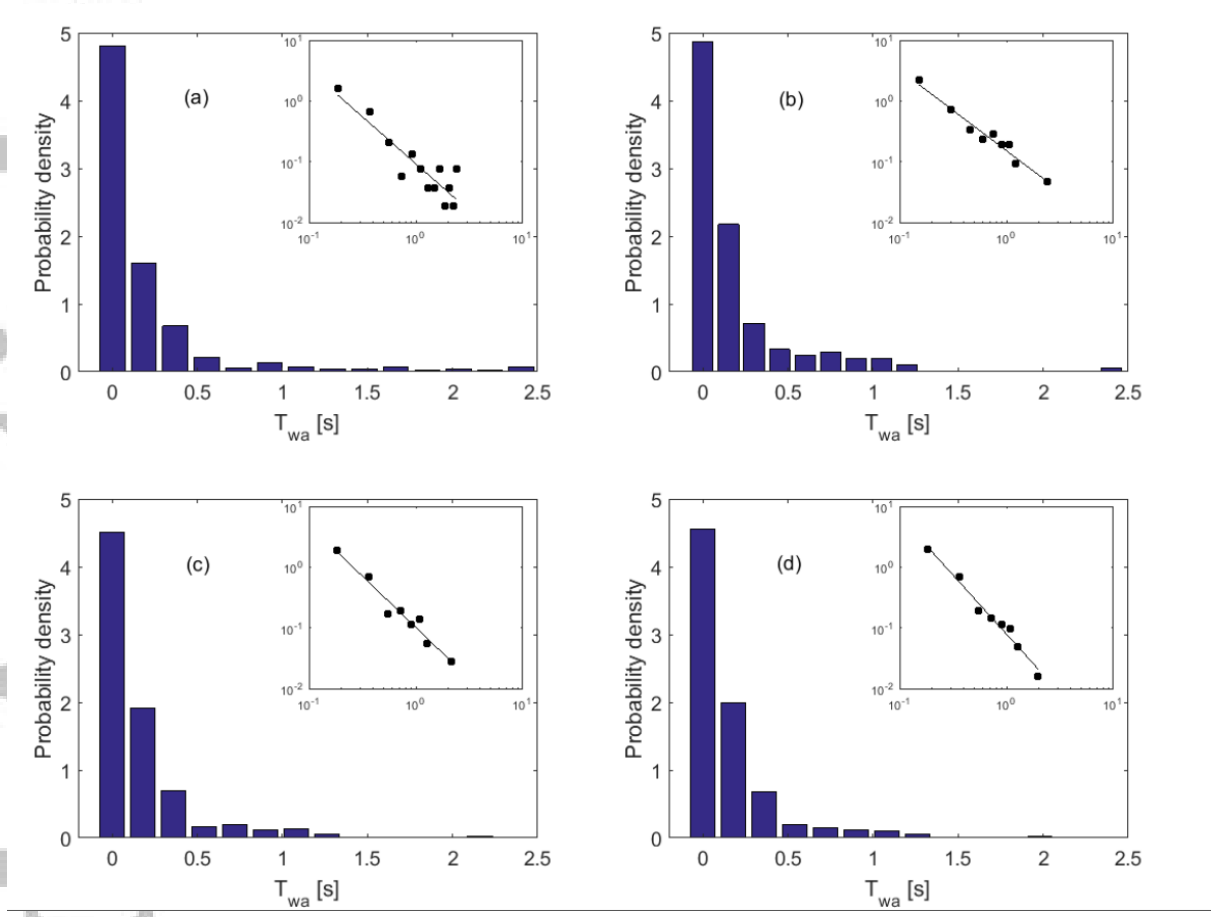

Figure 12. Distribution of active waiting time for the four experimental conditions S2 to S5 in panels (a) to (d), with power-law exponents estimated as -1.55, -1.33, -1.69 and -1.94, respectively. The form of the power law is provided in Equation (3).

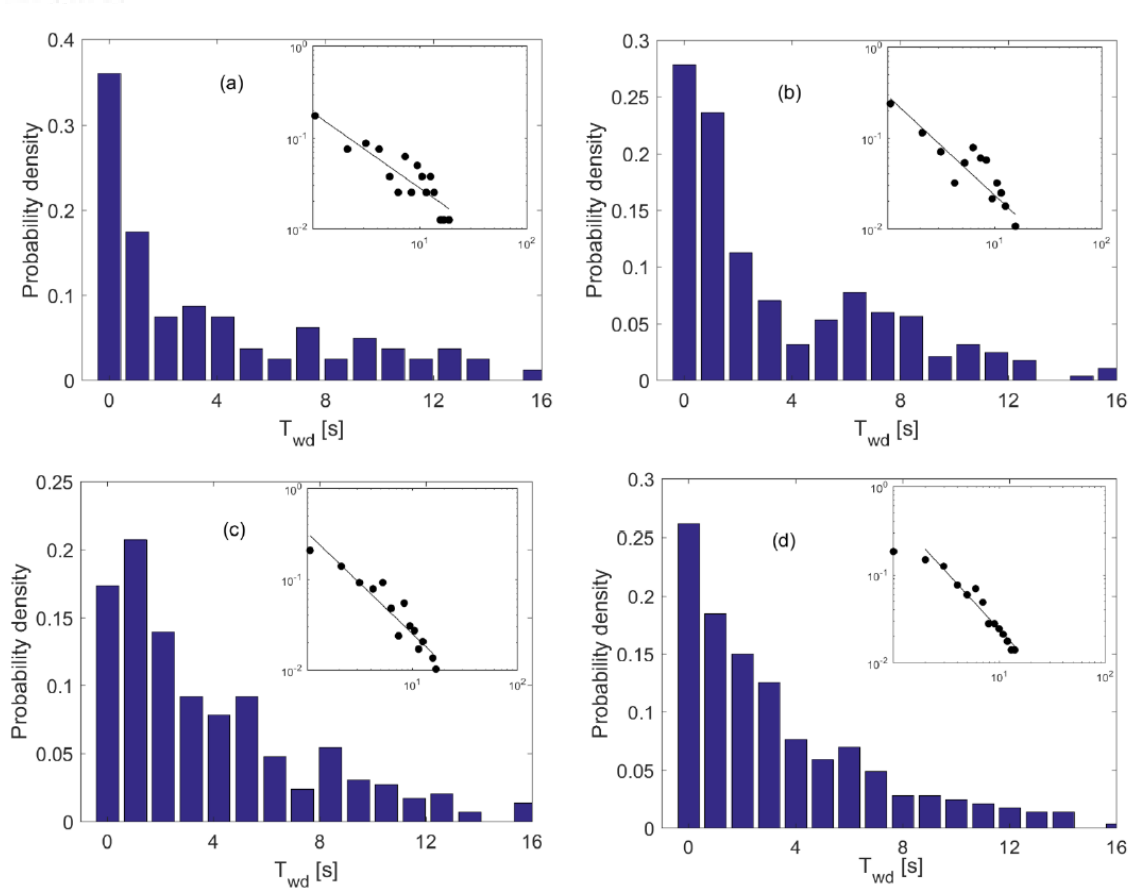

Figure 13. Distribution of the deep waiting time for the four experimental conditions S2 to S5 in panels (a) to (d). The form of the power law is provided in Equation (2). The exponent of four curve is -0.83, -1.09, -1.13, -1.32. The value of *a* is 0.19, 0.29, 0.33, 0.49.

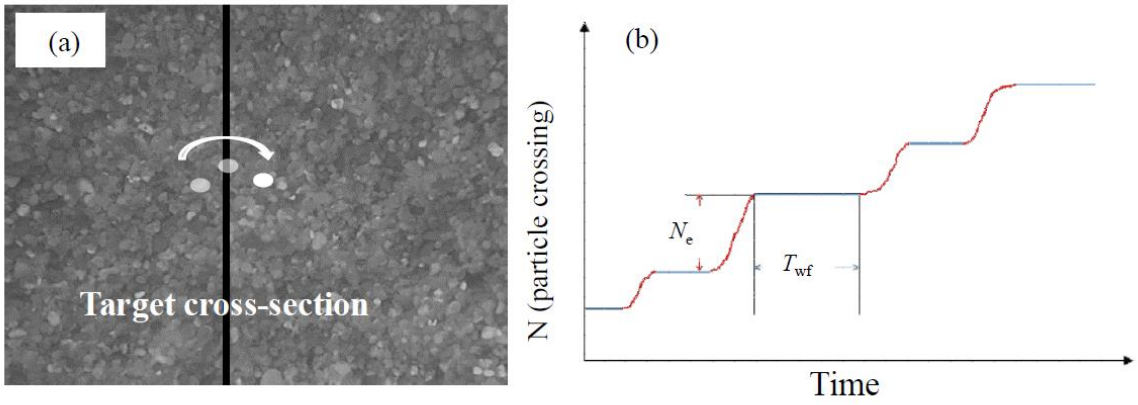

Figure 14. Sketch of the waiting time of the bed load flux T_{wf}. (a) N Particles crossing the target section during the transport event e, induce (b) dichotomic mass flux increase that are separated by the time T_{wf}.

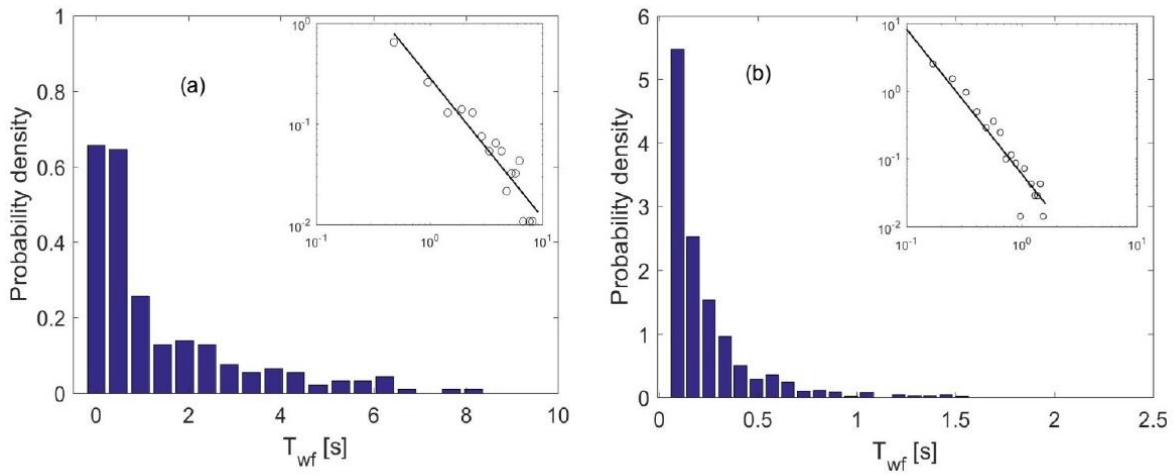

Figure 15. Distribution of the waiting time of bed load flux T_{wf} for the two experimental conditions S2 and S4 in panels (a) to (b), with power-law exponents estimated as -1.39 and -2.14, respectively. The PDF line is fitted in log-log scale, and the PDF form is provided in Equation (3).

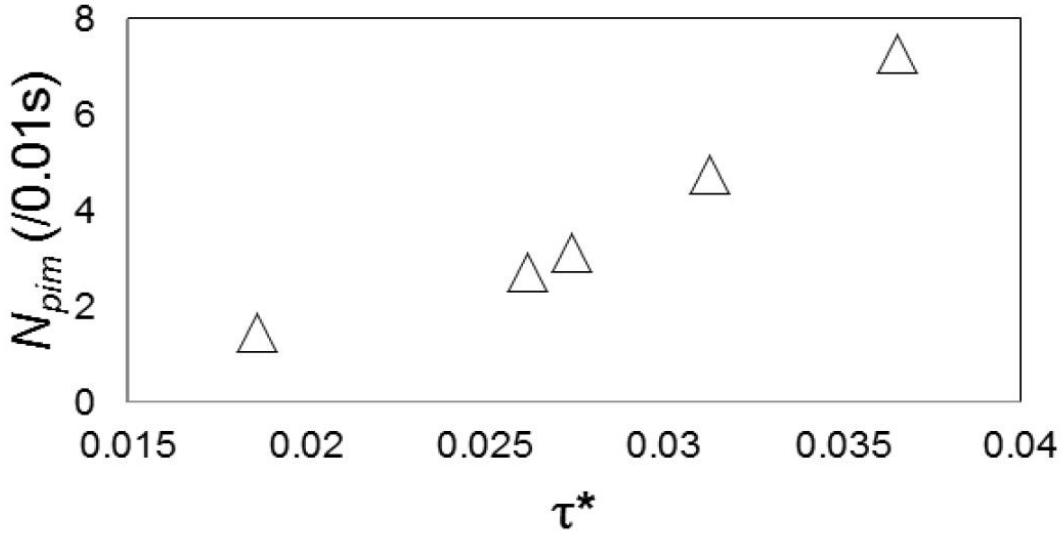

Figure 16. The number of the particles in motion N_{pim} on the bed surface as a function of the dimensionless shear stress τ*. N_{pim} is estimated in each frame (sample interval ~0.01s) over an area of (~7.3 cm × 5.5 cm), from the selected N_s trajectories (Table 2).